Thermodynamics of Salt Lake System: Representation, Experiments, and Visualization

Kui S. Kwok and Ka M. Ng
Dept. of Chemical Engineering, Hong Kong University of Science and Technology, Clear Water Bay, Kowloon, Hong Kong

Maria E. Taboada and Luis A. Cisternas
Dept. de Ingenieria Quimica, Universidad de Antofagasta, Casilla 170, Antofagasta, Chile

DOI 10.1002/aic.11421
Published online January 24, 2008 in Wiley InterScience (www.interscience.wiley.com).

A coherent, systematic approach for the determination of solid–liquid phase behavior of a multi-component salt lake system for use in the synthesis of crystallization process is presented. It centers on the thermodynamics of such a salt lake system and integrates three interrelated activities—representation of the system phase behavior as a phase diagram/thermodynamic model, experimental determination of the necessary data and visualization of the relevant crystallization regions. To illustrate this approach, the thermodynamics of a simplified salt lake system Li^+, Na^+, K^+, Mg^{2+}// Cl^-, SO_4^{2-} -H_2O at 25°C and 1 atm was determined. The identification of process alternatives using the resulting phase diagram for recovering $Li_2SO_4{\cdot}H_2O$ was also illustrated. © 2008 American Institute of Chemical Engineers *AIChE J,* 54: 706–727, 2008
Keywords: high-dimensional phase diagram, crystallization, thermodynamic model development, salt lake system, process design, solid–liquid equilibrium

Introduction

Inorganic salts have wide applications. For example, sodium chloride is a flavor enhancer for food and a deicing agent for highways in winter time; sodium sulfate serves as filler in detergent formulations; sodium carbonate is used in the manufacture of glass, and pulp and paper; potassium chloride is an important fertilizer; and lithium salts are the major source of lithium for batteries. They are plentiful in salt lakes, and crystallization-based techniques have been utilized to extract the desirable inorganic salts from them.[1–6] The normal practice is to pump the salt lake brine to a series of solar ponds where crystals of different salts are obtained successively through evaporative crystallization. For a feed with a given composition, the determination of which particular salt (or a mixture of salts) crystallizes under a specific set of operating conditions and the development of the corresponding crystallization-based extraction process requires knowledge of the solid–liquid equilibrium (SLE) phase behavior of the salt lake system and process design methods.

While process synthesis procedures based on SLE phase diagrams are well-established[7–9] and optimization methods have been proposed,[10–13] a salt lake system poses special challenges. First, with a large number of electrolytes, a high-dimensional phase diagram is required for complete representation of the phase behavior. Clearly, such a diagram cannot be drawn on a piece of paper and has to go hand-in-hand with a thermodynamic model. Second, again, because of the large number of components, it is often found that the desirable solubility data simply do not exist. While sometimes such information may be obtained from databases or commercial simulators,[14,15] the degree of accuracy and reliability required for designing a commercial plant inevitably become an issue. This problem is compounded by the presence of

Correspondence concerning this article should be addressed to K. M. Ng at kekmng@ust.hk.

Table 1. List of Components Included in the Present Study

No.	Name	Formula/Composition
	Solvent	
1	Water	H_2O
	Cations	
2	Lithium ion	Li^+
3	Sodium ion	Na^+
4	Potassium ion	K^+
5	Magnesium ion	Mg^{2+}
	Anions	
6	Chloride ion	Cl^-
7	Sulfate ion	SO_4^{2-}
	Salts (1 Cation + 1 Anion)	
8	Halite	NaCl
9	Thenardite	Na_2SO_4
10	Sylvite	KCl
11	Potassium sulfate	K_2SO_4
12	Mirabilite (Glauber salt)	$Na_2SO_4{\cdot}10H_2O$
13	Bischofite	$MgCl_2{\cdot}6H_2O$
14	Kieserite	$MgSO_4{\cdot}H_2O$
15	Hexahydrite	$MgSO_4{\cdot}6H_2O$
16	Epsomite	$MgSO_4{\cdot}7H_2O$
17	Lithium chloride monohydrate	$LiCl.H_2O$
18	Lithium sulfate monohydrate	$Li_2SO_4{\cdot}H_2O$
	Salts (2 Cations + 1 Anion)	
19	Glaserite	$Na_2SO_4{\cdot}3K_2SO_4$
20	Carnallite	$KCl.\ MgCl_2{\cdot}6H_2O$
21	Astrakanite	$Na_2SO_4{\cdot}MgSO_4{\cdot}4H_2O$
22	Schoenite	$K_2SO_4{\cdot}MgSO_4{\cdot}6H_2O$
23	Leonite	$K_2SO_4{\cdot}MgSO_4{\cdot}4H_2O$
24	Li-Carnallite	$LiCl.MgCl_2{\cdot}7H_2O$
25	Lithium double salt – 1	$Li_2SO_4{\cdot}3Na_2SO_4{\cdot}12H_2O$
26	Lithium double salt – 2	$Li_2SO_4{\cdot}Na_2SO_4$
27	Lithium double salt – 3	$Li_2SO_4{\cdot}K_2SO_4$
	Salts (2 Cations + 2 Anions)	
28	Kainite	$KCl.\ MgSO_4{\cdot}3H_2O$

numerous double salts and hydrates, existence of which cannot be accurately predicted by any theory. Thus, SLE experiments have to be performed alongside process synthesis. Third, even if a high-dimensional phase diagram captured in a thermodynamic model is available, it is non-trivial to design a process based on 2D cuts and projections of such a high-dimensional phase diagram. It is crucial that the design engineer be able to identify the crystallization regions and trace the solid and liquid process paths on them.[16]

The objective of this article is to show how these challenges can be met in a coherent, systematic manner by extending and integrating various existing methods. To be concrete, we focus on a model aqueous system consisting of four cations and two anions although the methodology is expected to be generally applicable to any salt lake system, and indeed to any multicomponent aqueous electrolyte system. We begin with a general discussion of the mathematical and graphical representation of the phase behavior of salt lake systems. Then, we show how the phase behavior can be constructed through systematic experimental determination of any missing solubility data and thermodynamic regression of all the available data. Finally, we demonstrate visualization of the phase diagram through projections and cuts as well as how such visualization process can aid the process synthesis activities.

The Salt Lake System

We focus on an isothermal-isobaric aqueous system comprising Li^+, Na^+, K^+, Mg^{2+}, Cl^-, and SO_4^{2-} ions at 25°C and 1 atm, which is characteristic of salt lake brines containing relatively high content of lithium, such as those in the Salar de Atacama of Chile.[17] A complete listing of the components involved in this system is provided in Table 1. As listed, this aqueous system of four cations and two anions can form 21 stable salts in various forms (simple salts, multiple salts, and hydrates) at 25°C and 1 atm. These salts are classified based on the number of their constituent cations and anions. Any of these salts can crystallize from the aqueous solution depending on the composition of the solution, and the operating temperature and pressure.

Representation of Phase Behavior

The knowledge of solid–liquid phase behavior of a salt lake system should be represented properly to facilitate the determination of which salts will crystallize under the given operating conditions and also the synthesis of the corresponding crystallization-based processes. For such a representation, two components are required:

Table 2. Experimental Procedures for the Isothermal Solid-Disappearance Method and the Analytical Method

Steps	Description
	Isothermal Solid-Disappearance Method (adopted by Hong Kong authors)
1	A sample mixture of salts of known composition was weighed into the inner tube of a jacketed glass vessel. A small amount of water was then added to the salt mixture such that excess solids remained in the aqueous solution
2	The sample was maintained at 25°C using a water bath connected to the outer tube of the jacketed glass vessel (Figure 1a). A magnetic stirrer was used to provide vigorous agitation to the sample
3	After 24 hours, a known mass of water was added to the sample through the septum using the gas-tight syringe every 1 hour. When the sample approached equilibrium, as indicated by decreased turbidity, the amount of water added was reduced and the duration between additions was increased to 5 hours
4	When the last trace of salts was observed to disappear and a clear solution was obtained, the total amount of water added was noted
5	The saturation composition at 25°C was calculated from the initial amount of salts weighed and the total mass of water added
	Analytical Method (adopted by Chilean authors)
1	Two identical aqueous samples containing excess salts were prepared in 22-ml flasks
2	The flasks were shaken for 3 days in a temperature bath maintained at 25°C (Figure 1b). This duration was deemed sufficient for samples to attain equilibrium in preliminary solubility studies
3	The samples were allowed to settle for 4 hours. The clear liquid samples were drawn with syringes and the solids were separated from the solution by filtration
4	Concentrations of Li^+ and Mg^{2+} in the liquid samples were measured using a double beam atomic absorption spectrometer, whereas concentrations of Cl^- and SO_4^{2-} in the liquid samples were determined by the Mohr method and the gravimetric method, respectively
5	The identities of the collected solids were analyzed by X-ray diffraction
6	Results from the two identical experiments were compared and only the comparable results were retained

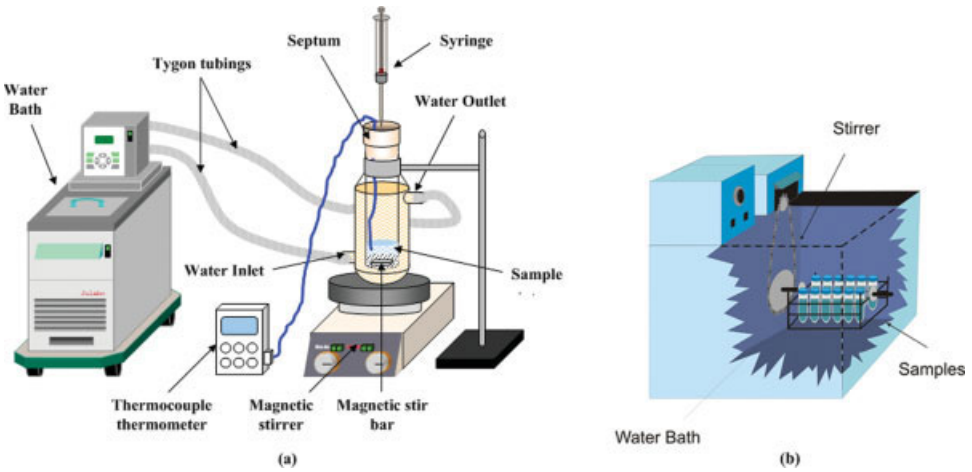

Figure 1. Experimental setup for (a) the isothermal solid-disappearance method and (b) the analytical method.

[Color figure can be viewed in the online issue, which is available at www.interscience.wiley.com.]

Table 3. Pros and Cons of the Isothermal Solid-Disappearance Method and the Analytical Method

	Isothermal Solid Disappearance Method	Analytical Method
Pros	• Very inexpensive and considerably less rigorous • Initial weight measurements are more reliable	• Identifies the saturated salts at the end of the experiments • Very useful for measuring double/multiple saturation varieties
Cons	• Requires knowledge of the saturated salts • Not very reliable for measuring double/multiple saturation varieties	• Expensive and considerably more rigorous • Techniques used for measuring the liquid and solid phase compositions may add to experimental error

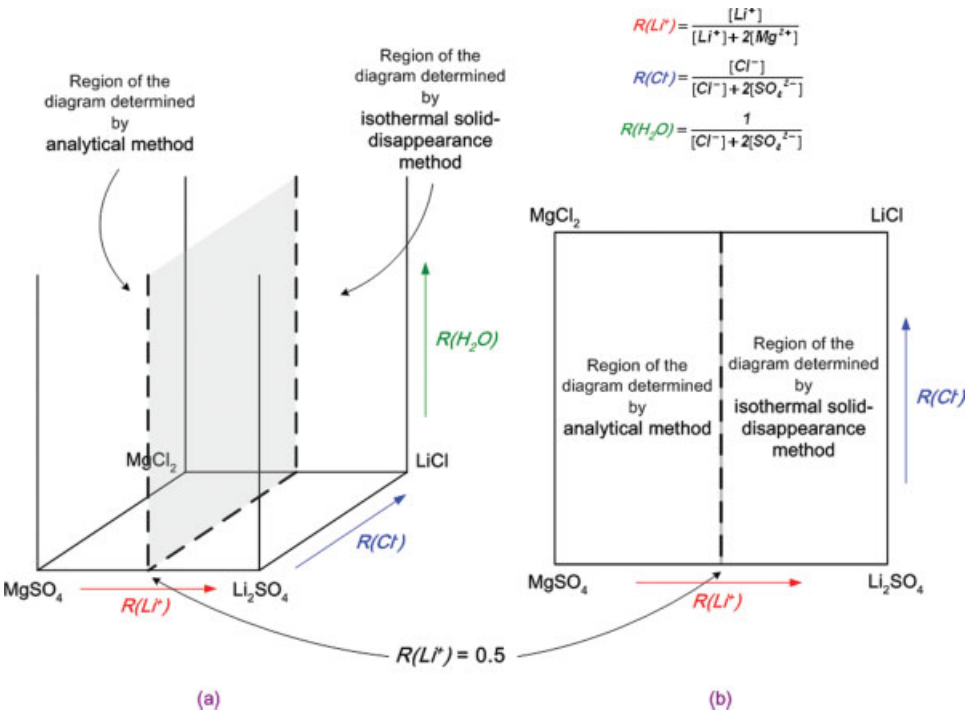

Figure 2. Regions of the phase diagram that are respectively determined by the isothermal solid-disappearance method and the analytical method—illustration using (a) the 3D phase diagram and (b) the corresponding 2D image after subjected to orthogonal projection.

[Color figure can be viewed in the online issue, which is available at www.interscience.wiley.com.]

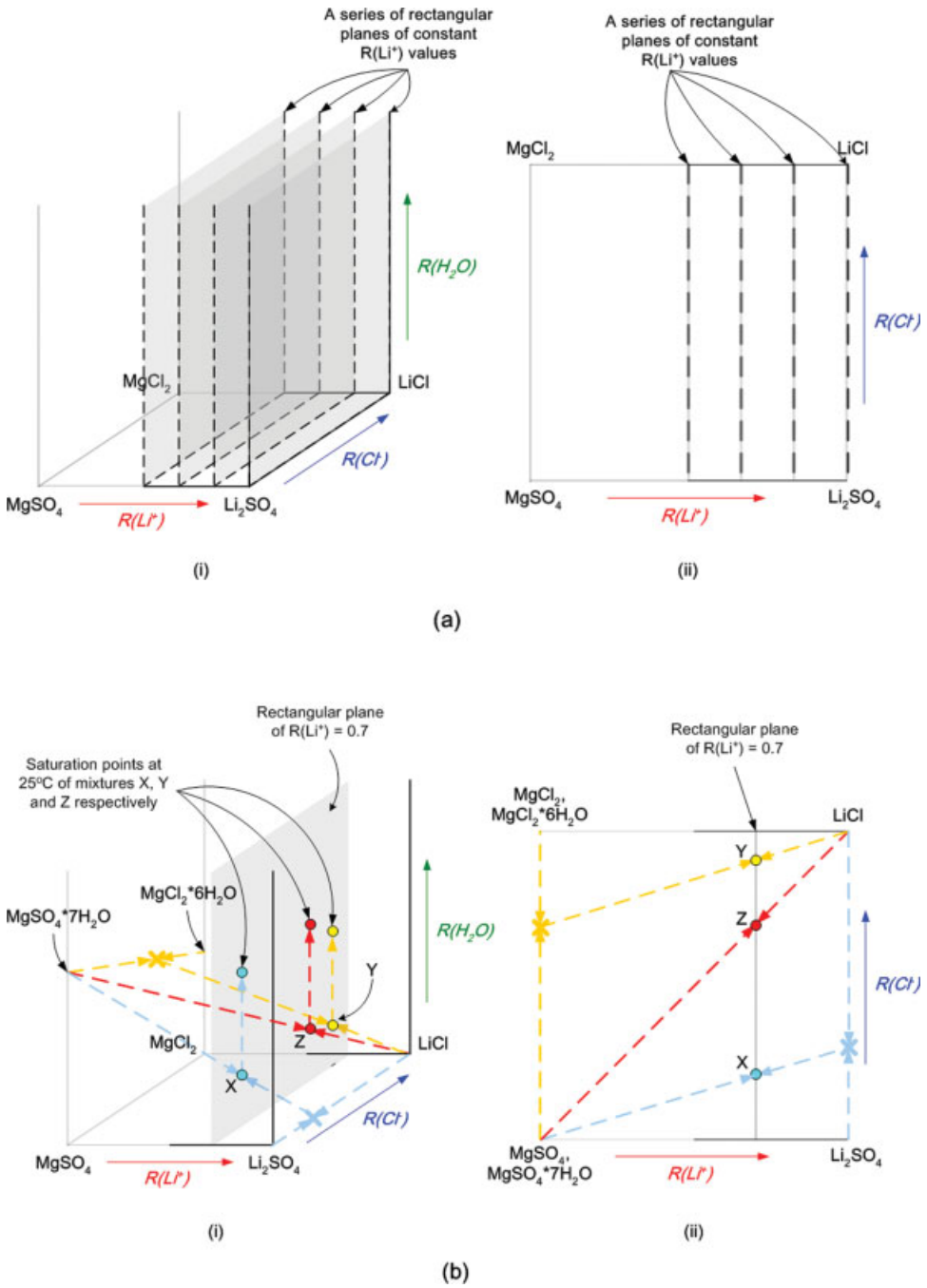

Figure 3. The experimental scheme formulated to determine the solid–liquid saturation curves for the region $0.5 \leq R(Li^+) \leq 1$ of the phase diagram: (a) Division of the phase diagram into a series of planes carrying constant values of $R(Li^+)$; (b) The strategies used to prepare samples of different solvent-less compositions.

The illustrations are given in two views: (i) 3D phase diagram and (ii) the corresponding 2D image after subjected to orthogonal projection. [Color figure can be viewed in the online issue, which is available at www.interscience.wiley.com.]

- A thermodynamically consistent mathematical model to calculate the phase behavior for any set of operating conditions.
- A coordinate scheme and a systematic method for taking projections and cuts to graphically visualize the calculated phase behavior.

Thermodynamic model

A thermodynamic model is needed for the mathematical representation of the solid–liquid phase behavior of the salt lake system. We are primarily interested in being able to identify all liquid compositions at which the various salts

Table 4. Experimental Solubility Data Obtained for the Subsystem Li^+, Mg^{2+}//Cl^-, SO_4^{2-}-H_2O at 25°C and 1 atm Using the Isothermal Solid-Disappearance Method

	Composition of Saturated Solution (wt %)				Transformed Coordinate Values		
Experimental Data for	Li^+	Mg^{2+}	Cl^-	SO_4^{2-}	$R(Li^+)$	$R(Cl^-)$	$R(H_2O)$
$R(Li^+) = 1$	3.27	0.00	0.00	22.63	1.0000	0.0000	0.1573
	3.19	0.00	1.61	19.91	1.0000	0.0985	0.1637
	3.10	0.00	3.32	16.95	1.0000	0.2099	0.1715
	3.08	0.00	4.81	14.82	1.0000	0.3057	0.1740
	3.04	0.00	6.19	12.64	1.0000	0.3990	0.1785
	3.02	0.00	8.09	9.92	1.0000	0.5248	0.1817
	3.02	0.00	9.65	7.82	1.0000	0.6259	0.1828
	3.12	0.00	12.10	5.18	1.0000	0.7600	0.1772
	3.07	0.00	11.93	5.09	1.0000	0.7606	0.1805
	3.26	0.00	14.84	2.45	1.0000	0.8912	0.1691
	3.62	0.00	17.58	1.23	1.0000	0.9510	0.1487
	3.94	0.00	19.64	0.67	1.0000	0.9756	0.1334
	4.13	0.00	20.77	0.44	1.0000	0.9846	0.1254
	4.40	0.00	22.29	0.24	1.0000	0.9921	0.1153
	4.61	0.00	23.44	0.17	1.0000	0.9948	0.1080
	4.88	0.00	24.86	0.10	1.0000	0.9969	0.0997
	4.91	0.00	25.03	0.10	1.0000	0.9971	0.0988
	5.24	0.00	26.71	0.06	1.0000	0.9983	0.0901
	5.22	0.00	26.60	0.06	1.0000	0.9985	0.0906
	5.70	0.00	29.08	0.05	1.0000	0.9988	0.0793
	7.60	0.00	38.77	0.05	1.0000	0.9990	0.0490
	5.85	0.00	29.83	0.04	1.0000	0.9991	0.0763
	7.10	0.00	36.26	0.03	1.0000	0.9993	0.0553
	7.62	0.00	38.91	0.03	1.0000	0.9994	0.0487
	7.59	0.00	38.76	0.03	1.0000	0.9995	0.0490
	7.63	0.00	38.97	0.02	1.0000	0.9997	0.0485
	7.53	0.00	38.45	0.00	1.0000	1.0000	0.0498
	7.58	0.00	38.72	0.00	1.0000	1.0000	0.0492
$R(Li^+) = 0.85$	2.93	0.90	0.00	23.83	0.8502	0.0000	0.1458
	2.92	0.91	0.00	23.82	0.8496	0.0000	0.1459
	2.92	0.90	0.00	23.79	0.8500	0.0000	0.1461
	2.85	0.88	1.84	20.70	0.8500	0.1073	0.1528
	2.86	0.88	1.87	20.72	0.8503	0.1087	0.1522
	2.82	0.87	2.54	19.53	0.8501	0.1499	0.1552
	2.79	0.86	3.40	18.09	0.8505	0.2032	0.1584
	2.76	0.85	3.40	17.88	0.8501	0.2048	0.1604
	2.74	0.84	5.18	15.31	0.8505	0.3142	0.1634
	2.75	0.85	5.54	14.84	0.8503	0.3360	0.1634
	2.73	0.84	7.01	12.70	0.8503	0.4280	0.1659
	2.72	0.84	7.13	12.50	0.8499	0.4360	0.1665
	2.72	0.84	7.95	11.33	0.8502	0.4873	0.1677
	2.72	0.84	8.95	9.99	0.8502	0.5485	0.1683
	2.73	0.84	10.36	8.20	0.8502	0.6313	0.1682
	2.78	0.86	12.41	5.82	0.8501	0.7427	0.1658
	2.80	0.87	13.15	5.01	0.8501	0.7805	0.1644
	2.85	0.88	14.12	4.10	0.8501	0.8235	0.1614
	2.90	0.90	14.79	3.54	0.8500	0.8500	0.1586
	2.88	0.89	14.69	3.51	0.8501	0.8501	0.1601
	3.02	0.93	16.41	2.38	0.8499	0.9034	0.1508
	3.04	0.94	16.79	2.04	0.8497	0.9176	0.1496
	3.18	0.98	18.09	1.42	0.8500	0.9453	0.1414
	3.34	1.03	19.36	0.96	0.8502	0.9648	0.1330
	3.52	1.09	20.74	0.59	0.8501	0.9794	0.1240
	3.70	1.14	21.97	0.36	0.8502	0.9881	0.1161
	3.97	1.23	23.72	0.19	0.8501	0.9940	0.1053
	4.21	1.30	25.23	0.11	0.8500	0.9967	0.0969
	4.43	1.37	26.59	0.07	0.8500	0.9981	0.0899
	4.70	1.45	28.18	0.05	0.8499	0.9987	0.0824
	5.08	1.57	30.48	0.03	0.8499	0.9993	0.0730
	5.49	1.70	32.98	0.02	0.8501	0.9995	0.0643
	6.20	1.92	37.23	0.02	0.8500	0.9996	0.0520
	6.19	1.92	37.21	0.02	0.8499	0.9997	0.0521
	6.19	1.92	37.22	0.02	0.8499	0.9997	0.0520
	6.15	1.90	36.96	0.00	0.8503	1.0000	0.0527
	6.15	1.90	36.97	0.00	0.8500	1.0000	0.0527
	6.15	1.91	36.97	0.00	0.8492	1.0000	0.0527
	6.20	1.92	37.25	0.00	0.8500	1.0000	0.0520

Table 4. Continued

Experimental Data for	Composition of Saturated Solution (wt %)				Transformed Coordinate Values		
	Li^+	Mg^{2+}	Cl^-	SO_4^{2-}	$R(Li^+)$	$R(Cl^-)$	$R(H_2O)$
$R(Li^+) = 0.7$	2.54	1.91	0.00	25.14	0.6997	0.0000	0.1345
	2.54	1.91	0.00	25.10	0.6995	0.0000	0.1348
	2.50	1.88	1.11	23.22	0.7001	0.0610	0.1385
	2.49	1.87	1.84	22.12	0.7005	0.1011	0.1399
	2.45	1.84	2.78	20.49	0.7002	0.1552	0.1434
	2.46	1.84	3.68	19.29	0.7000	0.2056	0.1439
	2.42	1.81	4.48	17.83	0.7003	0.2541	0.1475
	2.40	1.80	5.90	15.72	0.7003	0.3372	0.1503
	2.39	1.79	6.34	15.05	0.7000	0.3635	0.1512
	2.38	1.79	7.88	12.86	0.6998	0.4535	0.1533
	2.36	1.77	8.35	12.06	0.7003	0.4840	0.1551
	2.38	1.78	9.73	10.32	0.7004	0.5610	0.1549
	2.37	1.78	9.92	9.96	0.7000	0.5743	0.1559
	2.39	1.79	11.67	7.81	0.7000	0.6693	0.1553
	2.39	1.80	12.22	7.10	0.6999	0.6999	0.1553
	2.40	1.80	12.28	7.12	0.7004	0.7004	0.1544
	2.41	1.81	12.84	6.40	0.6999	0.7310	0.1544
	2.47	1.86	14.88	4.31	0.6999	0.8237	0.1501
	2.62	1.96	17.34	2.37	0.7004	0.9084	0.1406
	2.76	2.08	19.15	1.38	0.6999	0.9494	0.1311
	2.90	2.18	20.59	0.82	0.6998	0.9714	0.1229
	3.08	2.31	22.10	0.47	0.7000	0.9846	0.1138
	3.21	2.41	23.21	0.31	0.6999	0.9902	0.1071
	3.40	2.55	24.65	0.18	0.7000	0.9946	0.0990
	3.70	2.78	26.94	0.08	0.6999	0.9979	0.0873
	3.83	2.87	27.87	0.06	0.7000	0.9984	0.0830
	4.08	3.07	29.76	0.04	0.6997	0.9991	0.0750
	4.33	3.25	31.59	0.03	0.6998	0.9994	0.0682
	4.48	3.36	32.67	0.02	0.7000	0.9995	0.0645
	4.72	3.54	34.45	0.02	0.7000	0.9996	0.0589
	4.73	3.55	34.50	0.02	0.7000	0.9996	0.0588
	4.71	3.54	34.36	0.00	0.6996	1.0000	0.0592
$R(Li^+) = 0.55$	2.12	3.03	0.00	26.66	0.5508	0.0000	0.1228
	2.11	3.01	0.00	26.48	0.5503	0.0000	0.1240
	2.07	2.96	1.60	23.85	0.5501	0.0833	0.1283
	2.08	2.98	2.20	23.18	0.5503	0.1139	0.1278
	2.03	2.91	3.39	20.97	0.5504	0.1796	0.1329
	2.04	2.91	4.22	19.87	0.5509	0.2236	0.1332
	2.02	2.89	4.25	19.66	0.5509	0.2267	0.1344
	2.01	2.87	5.29	18.05	0.5505	0.2844	0.1367
	2.01	2.88	6.36	16.65	0.5497	0.3411	0.1370
	2.00	2.86	6.37	16.53	0.5506	0.3430	0.1379
	1.98	2.83	7.68	14.44	0.5506	0.4190	0.1412
	1.98	2.83	8.27	13.71	0.5506	0.4496	0.1411
	1.97	2.82	9.26	12.23	0.5504	0.5063	0.1429
	1.98	2.84	10.11	11.21	0.5500	0.5500	0.1424
	1.97	2.82	10.04	11.13	0.5500	0.5500	0.1438
	1.97	2.83	10.46	10.63	0.5500	0.5713	0.1435
	1.98	2.83	11.82	8.86	0.5501	0.6440	0.1439
	2.01	2.88	13.72	6.67	0.5499	0.7360	0.1421
	2.06	2.95	15.90	4.41	0.5501	0.8301	0.1382
	2.15	3.08	18.05	2.63	0.5501	0.9029	0.1314
	2.24	3.21	19.53	1.68	0.5499	0.9402	0.1252
	2.39	3.42	21.59	0.84	0.5504	0.9722	0.1145
	2.56	3.66	23.46	0.41	0.5502	0.9872	0.1043
	2.77	3.96	25.56	0.18	0.5500	0.9949	0.0932
	2.89	4.14	26.75	0.11	0.5503	0.9969	0.0874
	3.00	4.30	27.80	0.08	0.5501	0.9980	0.0825
	3.12	4.48	28.97	0.05	0.5500	0.9987	0.0774
	3.22	4.61	29.85	0.04	0.5502	0.9990	0.0739
	3.28	4.71	30.46	0.03	0.5498	0.9992	0.0715
	3.40	4.87	31.57	0.02	0.5503	0.9994	0.0675
	3.39	4.85	31.48	0.00	0.5505	1.0000	0.0679
$R(Li^+) = 0.4$	1.51	3.98	0.00	26.20	0.4001	0.0000	0.1252
	1.48	3.89	2.80	21.86	0.4005	0.1481	0.1310
	1.47	3.86	5.53	17.96	0.4002	0.2943	0.1343
	1.48	3.87	6.39	16.86	0.4002	0.3392	0.1344
	1.48	3.88	7.55	15.34	0.4002	0.4002	0.1347

Table 4. Continued

Experimental Data for	Composition of Saturated Solution (wt %)				Transformed Coordinate Values		
	Li^+	Mg^{2+}	Cl^-	SO_4^{2-}	$R(Li^+)$	$R(Cl^-)$	$R(H_2O)$
	1.48	3.88	7.54	15.32	0.4002	0.4002	0.1350
	1.48	3.90	7.98	14.84	0.3997	0.4214	0.1345
	1.50	3.95	9.37	13.31	0.3998	0.4881	0.1327
	1.52	4.00	10.32	12.33	0.3998	0.5314	0.1311
	1.53	4.02	10.56	12.13	0.3999	0.5412	0.1303
	1.53	4.03	10.95	11.69	0.4001	0.5593	0.1300
	1.53	4.03	11.12	11.46	0.4001	0.5678	0.1301
	1.53	4.04	11.65	10.78	0.3993	0.5942	0.1303
	1.54	4.05	12.91	9.15	0.3998	0.6565	0.1305
	1.54	4.05	13.10	8.89	0.3995	0.6664	0.1305
	1.55	4.06	13.73	8.13	0.4003	0.6960	0.1303
	1.58	4.14	16.03	5.58	0.4003	0.7957	0.1279
	1.62	4.26	17.93	3.76	0.3997	0.8659	0.1240
	1.70	4.48	20.31	1.98	0.3996	0.9329	0.1165
	1.78	4.68	21.82	1.26	0.4005	0.9590	0.1098
	1.86	4.87	23.16	0.71	0.4003	0.9779	0.1039
	1.94	5.10	24.47	0.42	0.4001	0.9876	0.0974
	2.05	5.39	26.05	0.18	0.4000	0.9950	0.0898
	2.20	5.79	28.05	0.10	0.4000	0.9973	0.0805
	2.24	5.88	28.53	0.09	0.4000	0.9978	0.0784
	2.30	6.05	29.33	0.07	0.3998	0.9983	0.0751
	2.32	6.10	29.61	0.05	0.3997	0.9989	0.0741
	2.32	6.09	29.59	0.00	0.4000	1.0000	0.0743
$R(Cl^-) = 1$	0.00	9.13	26.62	0.00	0.0000	1.0000	0.0856
	0.00	9.10	26.53	0.00	0.0000	1.0000	0.0860
	0.00	9.11	26.56	0.00	0.0000	1.0000	0.0859
	0.00	9.10	26.55	0.00	0.0000	1.0000	0.0859
	0.00	9.12	26.59	0.00	0.0000	1.0000	0.0857
	0.00	9.11	26.56	0.00	0.0000	1.0000	0.0859
	0.67	8.21	27.35	0.00	0.1248	1.0000	0.0827
	1.39	7.26	28.25	0.00	0.2508	1.0000	0.0792
	2.31	6.10	29.60	0.00	0.3985	1.0000	0.0742
	3.39	4.85	31.48	0.00	0.5505	1.0000	0.0679
	4.16	4.08	33.15	0.00	0.6414	1.0000	0.0627
	4.41	3.85	33.74	0.00	0.6676	1.0000	0.0609
	4.43	3.87	33.93	0.00	0.6676	1.0000	0.0603
	4.61	3.65	34.19	0.00	0.6882	1.0000	0.0597
	4.71	3.54	34.36	0.00	0.6996	1.0000	0.0592
	4.88	3.30	34.58	0.00	0.7213	1.0000	0.0587
	4.96	3.21	34.69	0.00	0.7300	1.0000	0.0584
	5.31	2.80	35.30	0.00	0.7691	1.0000	0.0568
	5.60	2.45	35.78	0.00	0.7999	1.0000	0.0557
	5.81	2.25	36.23	0.00	0.8186	1.0000	0.0545
	6.15	1.91	36.97	0.00	0.8492	1.0000	0.0527
	6.39	1.68	37.53	0.00	0.8693	1.0000	0.0514
	6.59	1.55	38.16	0.00	0.8817	1.0000	0.0499
	6.69	1.37	38.19	0.00	0.8950	1.0000	0.0499
	6.99	0.92	38.37	0.00	0.9300	1.0000	0.0496
	7.18	0.61	38.45	0.00	0.9538	1.0000	0.0496
	7.58	0.00	38.73	0.00	1.0000	1.0000	0.0491
	7.54	0.00	38.51	0.00	1.0000	1.0000	0.0497
	7.57	0.00	38.68	0.00	1.0000	1.0000	0.0493
	7.57	0.00	38.69	0.00	1.0000	1.0000	0.0492
	7.58	0.00	38.74	0.00	1.0000	1.0000	0.0491
	7.58	0.00	38.71	0.00	1.0000	1.0000	0.0492
$R(Cl^-) = 0$	0.00	5.36	0.00	21.19	0.0000	0.0000	0.1665
	0.32	5.04	0.00	22.17	0.1011	0.0000	0.1570
	0.67	4.72	0.00	23.29	0.1996	0.0000	0.1471
	0.86	4.53	0.00	23.88	0.2504	0.0000	0.1422
	1.07	4.36	0.00	24.64	0.3009	0.0000	0.1363
	1.51	3.98	0.00	26.20	0.4001	0.0000	0.1252
	1.80	3.75	0.00	27.29	0.4568	0.0000	0.1182
	1.85	3.69	0.00	27.40	0.4670	0.0000	0.1176
	1.89	3.59	0.00	27.22	0.4794	0.0000	0.1188
	2.11	3.01	0.00	26.48	0.5503	0.0000	0.1240
	2.11	3.01	0.00	26.48	0.5514	0.0000	0.1241
	2.54	1.91	0.00	25.10	0.6995	0.0000	0.1348
	2.92	0.91	0.00	23.82	0.8496	0.0000	0.1459
	3.27	0.00	0.00	22.63	1.0000	0.0000	0.1573

listed in Table 1 are saturated at 25°C and 1 atm. A salt is saturated in the aqueous solution when its solubility product is equal to the product of activities of its constituents (here the salts are strong electrolytes and are considered to dissociate completely into their constituents). For example, for a solution saturated with lithium sulfate monohydrate:

$$K^{\mathrm{I}}_{\mathrm{Li_2SO_4.H_2O}} = K^{\mathrm{SP}}_{\mathrm{Li_2SO_4.H_2O}}$$

$$\left(\gamma^*_{\mathrm{Li^+}}[\mathrm{Li^+}]\right)\left(\gamma^*_{\mathrm{SO_4^{2-}}}\left[\mathrm{SO_4^{2-}}\right]\right)^{1/2}(\gamma_{\mathrm{W}}x_{\mathrm{W}})^{1/2} = \exp\left[-\frac{1}{RT}\left(\mu^*_{\mathrm{Li^+}} + \frac{\mu^*_{\mathrm{SO_4^{2-}}}}{2} + \frac{\mu^o_{\mathrm{W}}}{2} - \frac{\mu^o_{\mathrm{Li_2SO_4.H_2O}}}{2}\right)\right] \quad (1)$$

Therefore, to calculate the solid–liquid phase behavior of the salt lake system and to determine which salts will crystallize in stable form at different operating conditions, we need to calculate the solubility products for all salts and the activities for all aqueous phase components.

Solubility products of the salts can be calculated from information on Gibbs free energies of formation as can be seen from the RHS of Eq. 1. Usually, however, in view of the large number of stable salts that can form in a salt lake, the following standard expression for solubility products is more useful:[18]

$$\ln K^{\mathrm{SP}}_i = A_i + \frac{B_i}{T} + C_i \ln T + D_i T \quad \forall i \in \text{Stable Salts} \quad (2)$$

The activities of the aqueous phase components can be calculated using a variation of the UNIQUAC model extended to apply to aqueous electrolytic systems.[19,20] In this model, there are three contributions to the activity coefficient of water and of the ions, viz., Debye-Hückel contribution, combinatorial contribution and residual contribution. The Debye-Hückel contribution accounts for nonideality because of long-range electrostatic forces in the solution, the combinatorial contribution accounts for the nonideality due to differences in shapes and sizes of different components in the solution, and the residual contribution accounts for the short-range interactions in the solution.

The complete set of equations for each of the contributions is listed in Appendix. From these equations we can note that to represent the combinatorial contributions, we need the UNIQUAC volume and area parameters (r_i and q_i) and to represent the residual contribution, we need energy parameters (τ_{ij}) given by:

$$\tau_{ij} = \exp\left(-\frac{a_{ij} + b_{ij}T}{RT}\right) \quad (3)$$

Therefore, for complete mathematical representation of the solid–liquid phase behavior of the salt lake system under consideration, the following parameters are required:

- Solubility product parameters A_i, B_i, C_i, and D_i for each salt from Table 1
- UNIQUAC shape/size parameters r_i and q_i for each ion from Table 1
- Binary interaction parameters a_{ij} and b_{ij} for pairs of aqueous phase components (ions and water) from Table 1

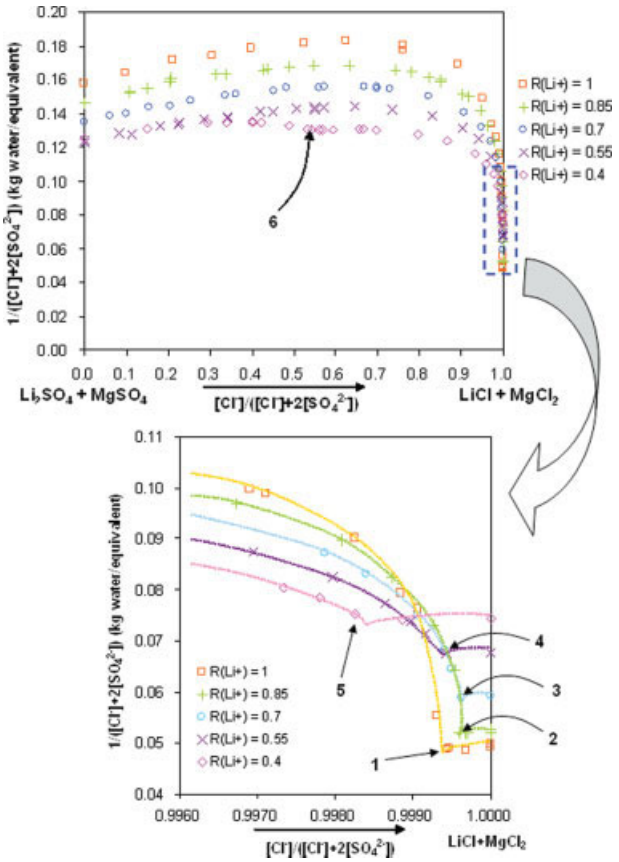

Figure 4. Solid–liquid saturation curves on certain planes of 0.4 ≤ R(Li^+) ≤ 1 in the phase diagram of the reciprocal subsystem Li^+, Mg^{2+}//Cl^-, SO_4^{2-} -H_2O at 25°C and 1 atm.

[Color figure can be viewed in the online issue, which is available at www.interscience.wiley.com.]

Determination of these parameters requires experimental solubility measurements and thermodynamic regression of the experimental data.

Note that the r and q parameters for water are not included in the list of parameters above but instead are fixed at 0.92 and 1.40, respectively. In reality, the r and q parameters for all components should be fixed based on molecular sizes. However, we found that fixing these values for the ions greatly affects the regression capability of the UNIQUAC model equations, especially as the number of ions and stable salts to be considered increases. Therefore, we have retained them in the list of parameters to be regressed.

Coordinate scheme, projections, and cuts

The number of independent coordinates F required for complete graphical representation of the isothermal-isobaric phase behavior of electrolytic systems is given as:[21,22]

$$F = m + n + i - 2 \quad (4)$$

where m represents the number of simple cations present in the system, n the number of simple anions, and i the number

Table 5. The Equilibrium Conditions of the Double Saturation Points Determined for the Region $0.5 \le R(Li^+) \le 1$ in the Phase Diagram of the Subsystem $Li^+, Mg^{2+}//Cl^-, SO_4^{2-}$-$H_2O$

Point	Composition of Saturated Solution (wt %)				Transformed Coordinate Values		Composition of Solid Phase
	Li^+	Mg^{2+}	Cl^-	SO_4^{2-}	$R(Li^+)$	$R(Cl^-)$	
1	7.62	0.00	38.91	0.03	1.0000	0.9994	$LiCl.H_2O + Li_2SO_4.H_2O$
2	6.20	1.92	37.23	0.02	0.8500	0.9996	$LiCl.MgCl_2.7H_2O + Li_2SO_4.H_2O$
3	4.72	3.54	34.45	0.02	0.7000	0.9996	$LiCl.MgCl_2.7H_2O + Li_2SO_4.H_2O$
4	3.40	4.87	31.57	0.02	0.5503	0.9994	$MgCl_2.6H_2O + Li_2SO_4.H_2O$
5	2.32	6.10	29.61	0.05	0.3997	0.9989	$MgCl_2.6H_2O + Li_2SO_4.H_2O$
6	1.53	4.02	10.56	12.13	0.3999	0.5412	$Li_2SO_4.H_2O + MgSO_4.7H_2O$

of non-dissociating molecular species or solvents. The term "simple ions" refers to those ions that cannot undergo any further dissociation in the solution to form other ions and for our model salt lake system includes all ions present.

There are several appropriate and consistent choices for expressing these F independent coordinates. We will use the following most convenient set:

- $m - 1$ coordinates related to compositions of simple cations (M_i):

$$R(M_i) = \frac{z_{M_i}[M_i]}{\sum_{j=1}^{m}(z_{M_j}[M_j])}, \quad i = 1, 2, \ldots, m-1 \tag{5}$$

- $n - 1$ coordinates related to compositions of simple anions (N_i):

$$R(N_i) = \frac{z_{N_i}[N_i]}{\sum_{j=1}^{n}(z_{N_j}[N_j])}, \quad i = 1, 2, \ldots, n-1 \tag{6}$$

- $i = 1$ coordinate related to the solvent:

$$R(H_2O) = \frac{1}{\sum_{j=1}^{m}(z_{M_j}[M_j])} = \frac{1}{\sum_{j=1}^{n}(z_{N_j}[N_j])} \tag{7}$$

where $R(M_i)$ and $R(N_i)$ are respectively the cationic equivalent fraction of cation M_i and the anionic equivalent fraction of anion N_i; $R(H_2O)$, the solvent coordinate, is the mass of solvent per equivalent of the salts; $[M_i]$ and $[N_i]$ are the molalities of cation M_i and anion N_i, respectively; z_{M_i} and z_{N_i} are the charge magnitudes of cation M_i and anion N_i respectively; m and n are the number of simple cations and anions in the system respectively.

Our salt lake system contains four cations (Li^+, Na^+, K^+, and Mg^{2+}), two anions (Cl^- and SO_4^{2-}) and one nondissociating molecular solvent H_2O. As a result, from Eq. 4, we have five independent coordinates. This implies that we cannot plot on paper the phase behavior in its entirety. However, it is still possible to generate various cuts and projections of the high dimensional phase diagram and plot them on pa-

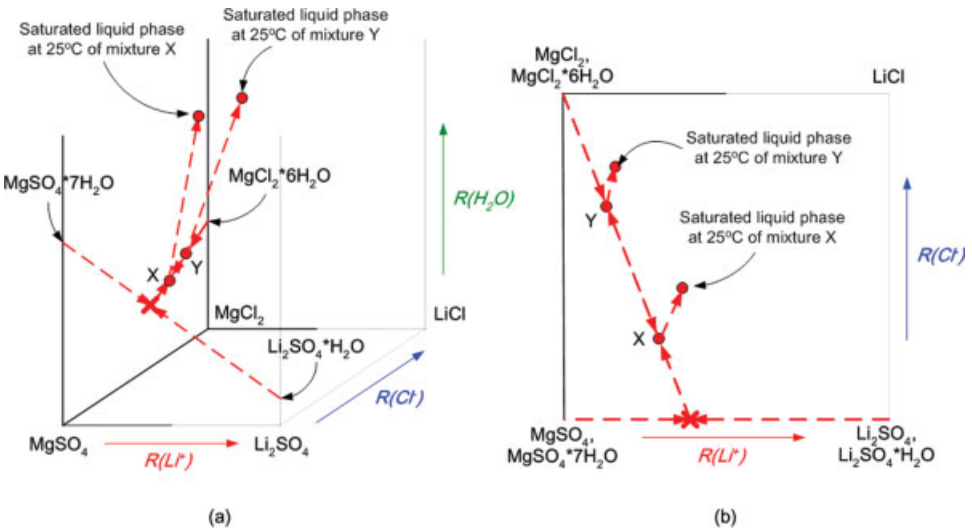

Figure 5. The experimental scheme formulated to determine the double or triple saturation points for the region $0 \le R(Li^+) \le 0.5$ of the phase diagram.

The illustrations are given in two views: (a) 3D phase diagram and (b) the corresponding 2D image after subjected to orthogonal projection. [Color figure can be viewed in the online issue, which is available at www.interscience.wiley.com.]

Table 6. The Equilibrium Conditions of the Double Saturation Points Determined for the Region $0 \le R(Li^+) \le 0.5$ in the Phase Diagram of the Subsystem Li^+, $Mg^{2+}//Cl^-$, SO_4^{2-}-H_2O

	Composition of Saturated Solution (wt %)				Transformed Coordinate Values		
Point	Li^+	Mg^{2+}	Cl^-	SO_4^{2-}	$R(Li^+)$	$R(Cl^-)$	Composition of Solid Phase
10	1.66	3.58	5.32	19.15	0.4481	0.2734	$MgSO_4.7H_2O + Li_2SO_4.H_2O$
	1.65	3.55	5.28	19.08	0.4487	0.2727	$MgSO_4.7H_2O + Li_2SO_4.H_2O$
11	1.42	4.02	11.93	10.34	0.3821	0.6098	$MgSO_4.7H_2O + Li_2SO_4.H_2O$
	1.42	4.02	11.88	10.36	0.3821	0.6084	$MgSO_4.7H_2O + Li_2SO_4.H_2O$
12	1.13	5.01	15.48	7.46	0.2831	0.7376	$MgSO_4.7H_2O + Li_2SO_4.H_2O$
	1.13	5.03	15.55	7.44	0.2823	0.7390	$MgSO_4.7H_2O + Li_2SO_4.H_2O$

per.[21–23] A projection is produced by not explicitly plotting the effect of one or more intensive variables on the phase behavior whereas a cut is generated by plotting the phase behavior at fixed values of one or more intensive variables. Each variable that is not explicitly considered or that is kept fixed reduces the dimensionality of the original phase diagram by one. For our salt lake system, we are interested in visualizing the phase behavior at a fixed temperature and pressure. Therefore, the only intensive variables that can be controlled are the composition variables for the solvent and the ions in the aqueous solution. For example, dimensionality of the phase diagram of our system can be reduced by one through plotting it as solvent-less projection created by ignoring the coordinate related to the solvent (Eq. 7). Further reduction in dimensionality can be achieved by plotting 2D projections of the solvent-less projection. Such 2D projections ignore the coordinate related to the solvent (Eq. 7) and only consider compositions of two specified cations and two specified anions in the cationic (Eq. 5) and anionic (Eq. 6) coordinates.

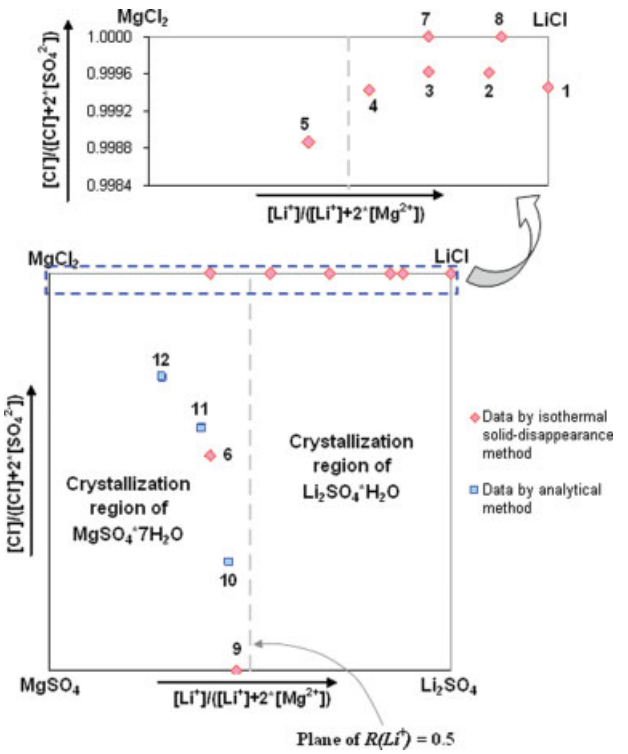

Figure 6. Two-dimensional solvent-less projection of the SLE phase diagram of the reciprocal subsystem Li^+, $Mg^{2+}//Cl^-$, SO_4^{2-}-H_2O at 25°C and 1 atm.

[Color figure can be viewed in the online issue, which is available at www.interscience.wiley.com.]

Determination of Phase Behavior

Let us turn our attention to determining the phase behavior of the salt lake system under investigation. The determination

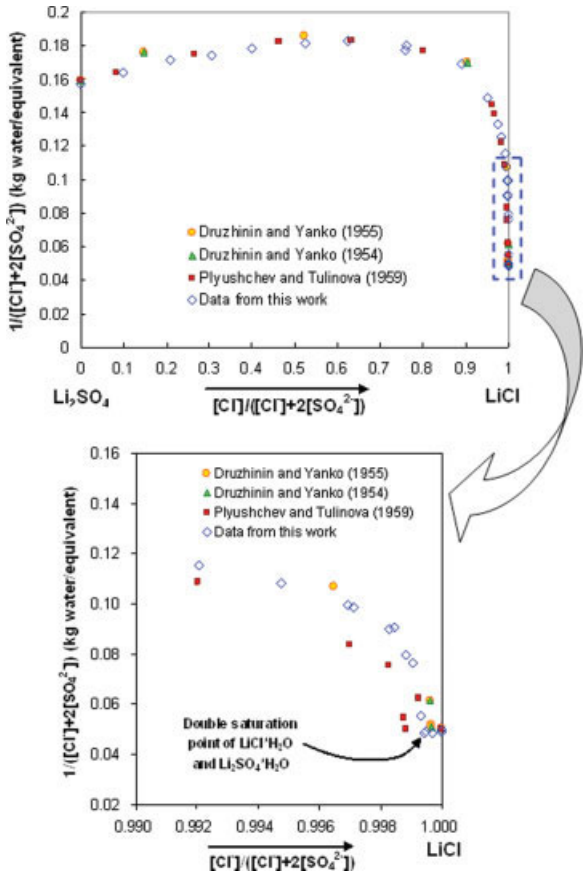

Figure 7. The solid–liquid saturation curve of system LiCl-Li_2SO_4-H_2O at 25°C and 1 atm.[24,48–50]

[Color figure can be viewed in the online issue, which is available at www.interscience.wiley.com.]

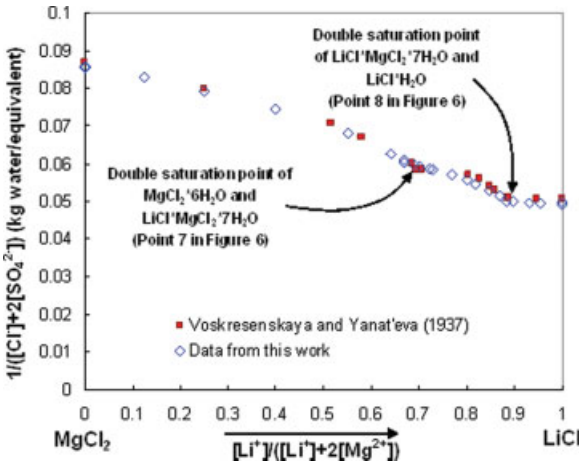

Figure 8. The solid–liquid saturation curve of system LiCl-$MgCl_2$-H_2O at 25°C and 1 atm.[24,51]

[Color figure can be viewed in the online issue, which is available at www.interscience.wiley.com.]

strategy and experimental procedures are first described, followed by the use of thermodynamic regression to generate the thermodynamic model parameters from the experimental data.

Determination strategy and experimental procedures

The only practical way to determine the phase behavior of the selected multi-component system is to break it down into a set of constituting subsystems of lower dimension and measure the solubility data for each of them. However, the data from these subsystems must be adequate to identify the important thermodynamic features of the original system. In particular, regions of liquid phase composition at which various salts from Table 1 will be saturated at 25°C and 1 atm need to be identified, since these regions, their boundaries and intersections make up the phase behavior of our salt lake system. It is required that, at the very least,

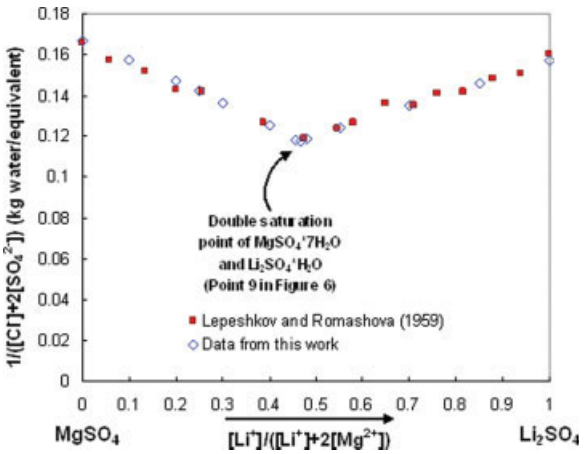

Figure 9. The solid–liquid saturation curve of system Li_2SO_4-$MgSO_4$-H_2O at 25°C and 1 atm.[52]

[Color figure can be viewed in the online issue, which is available at www.interscience.wiley.com.]

- Each aqueous phase component should be present along with every other aqueous component at least once
- Each stable salt should be saturated at least once

To fulfill these minimum requirements, we have to obtain solubility data for 6 quaternary subsystems, each of which is formed by the solvent water as well as a pair of cations and a pair of anions present in our salt lake system (e.g., Li^+, Na^+//Cl^-, SO_4^{2-} -H_2O and K^+, Mg^{2+}//Cl^-, SO_4^{2-} -H_2O). To the best of our knowledge, except for the reciprocal subsystem Li^+, Mg^{2+}//Cl^-, SO_4^{2-} -H_2O, reliable solubility data at 25°C and 1 atm of all subsystems are available from multiple sources.[24–44]

To determine the phase behavior of the reciprocal subsystem Li^+, Mg^{2+}//Cl^-, SO_4^{2-}-H_2O, we used two distinct experimental techniques[45–47] in this work:

- Isothermal solid-disappearance (synthetic) method (adopted by Hong Kong authors)
- Analytical method (adopted by Chilean authors).

Table 2 summarizes the experimental procedures for both methods. The corresponding experimental setups used are shown in Figures 1a and 1b respectively. As indicated in the procedures, the main difference between the two methods is that synthetic method relies on initial composition measurements while the analytical method measures the liquid phase compositions and determines the identities of the solid phases at the end of each experiment. Some selected pros and cons for the two methods are given in Table 3.

Table 7. Regressed UNIQUAC *r* and *q* Parameters and Salt Solubility Products at 25°C and 1 atm. (For water, *r* and *q* Values are Fixed at 0.92 and 1.40, Respectively)

	UNIQUAC Parameters	
Ion	*r*	*q*
Na^+	1.42527	1.03801
K^+	2.25833	1.83019
Mg^{2+}	1.68526	0.64027
Li^+	1.06576	1.29327
Cl^-	10.6729	10.2754
SO_4^{2-}	12.4237	12.1671

Salt		
Name	Formula	K^{SP} at 25°C
Halite	NaCl	3.82072
Thenardite	Na_2SO_4	−0.726922
Sylvite	KCl	2.20696
Potassium sulfate	K_2SO_4	−4.16601
Mirabilite (Glauber Salt)	$Na_2SO_4.10H_2O$	−2.92313
Bischofite	$MgCl_2.6H_2O$	11.413
Kieserite	$MgSO_4.H_2O$	−0.210492
Hexahydrite	$MgSO_4.6H_2O$	−3.75763
Epsomite	$MgSO_4.7H_2O$	−4.36396
Lithium chloride monohydrate	$LiCl.H_2O$	11.6441
Lithium sulfate monohydrate	$Li_2SO_4.H_2O$	2.52436
Glaserite	$Na_2SO_4.3K_2SO_4$	−18.0605
Carnallite	$KCl.MgCl_2.6H_2O$	11.3943
Astrakanite	$Na_2SO_4.MgSO_4.4H_2O$	−5.7959
Schoenite	$K_2SO_4.MgSO_4.6H_2O$	−10.3395
Leonite	$K_2SO_4.MgSO_4.4H_2O$	−9.562
Li-Carnallite	$LiCl.MgCl_2.7H_2O$	21.7264
Lithium Double Salt-1	$Li_2SO_4.3Na_2SO_4.12H_2O$	−6.56961
Lithium Double Salt-2	$Li_2SO_4.Na_2SO_4$	0.810216
Lithium Double Salt-3	$Li_2SO_4.K_2SO_4$	−4.82978
Kainite	$KCl.MgSO_4.3H_2O$	−0.4435

Table 8. Regressed UNIQUAC Interaction Parameters a_{ij} (All b_{ij} Parameters are Zero)

	Na^+	K^+	Mg^{2+}	Li^+	Cl^-	SO_4^{2-}	Water
Na^+	0.0	3.91767e+5	−1.05149e+6	1.24363e+5	−2.55173e+7	−7.28818e+6	4.16241e+6
K^+	3.91767e+5	0.0	−1.76315e+6	−3.13587e+6	−2.64615e+7	−8.46461e+6	−4.93552e+5
Mg^{2+}	−1.05149e+6	−1.76315e+6	0.0	9.01251e+6	−2.14966e+7	−6.22645e+6	1.31526e+7
Li^+	1.24363e+5	−3.13587e+6	9.01251e+6	0.0	−2.44032e+7	−6.9584e+6	7.40563e+5
Cl^-	2.38589e+6	1.44168e+6	6.40655e+6	3.49996e+6	0.0	6.7392e+6	3.82535e+6
SO_4^{2-}	2.80862e+6	1.63219e+6	3.87035e+6	3.1384e+6	−1.10672e+7	0.0	3.85226e+6
Water	4.16241e+6	−4.93552e+5	1.31526e+7	7.40563e+5	−2.40778e+7	−6.24454e+6	0.0

Figure 2a shows the coordinate scheme for graphical visualization of the subsystem Li^+, Mg^{2+}//Cl^-, SO_4^{2-} -H_2O in 3D and Figure 2b shows the orthogonal (solvent-less) projection of the same scheme in two-dimensions. In both figures, the composition space represented by the scheme is divided into two regions. Preliminary examination of phase behavior of relevant ternary systems (see section entitled additional experiments below) revealed that the region on the right ($0.5 \leq R(Li^+) \leq 1$) is almost entirely covered by the saturation region for lithium sulfate monohydrate. Saturation regions for lithium chloride monohydrate and for other chloride-containing salts lie extremely close to the top ($R(Cl^-) \sim 1$). For these reasons, rigorous analysis and identification of the solid and liquid phases can be avoided and the simpler isothermal solid–disappearance method was used for this region. On the other hand, the more rigorous analytical method was used for the region on the left ($0 \leq R(Li^+) \leq 0.5$) because of the presence of comparable saturation regions of magnesium and lithium salts.

Experiments for $0.5 \leq R(Li^+) \leq 1$. In this region, the isothermal solid-disappearance method was utilized for measuring solubilities on planes defined by different values of $R(Li^+)$. These planes are shown in Figure 3a. To prepare the initial sample mixture carrying a specific value of $R(Li^+)$ for solubility measurement, three different strategies were adopted depending on the solvent-less composition of the

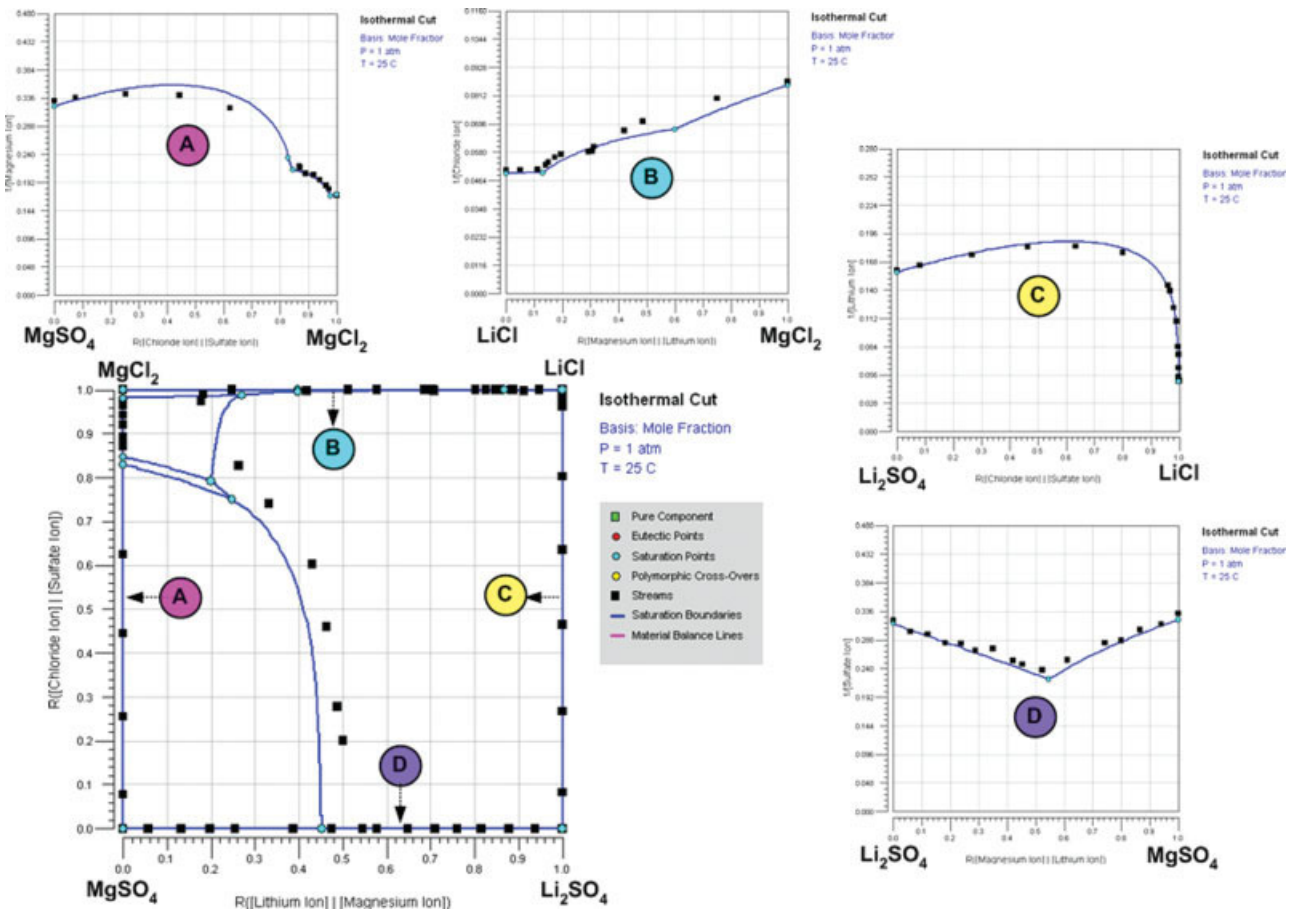

Figure 10. Comparison of calculated and experimental phase behavior for Li^+, Mg^{2+}//Cl^-, SO_4^{2-}-Water system.

Line - calculated phase behavior; Point - measured or literature data.[50–53] [Color figure can be viewed in the online issue, which is available at www.interscience.wiley.com.]

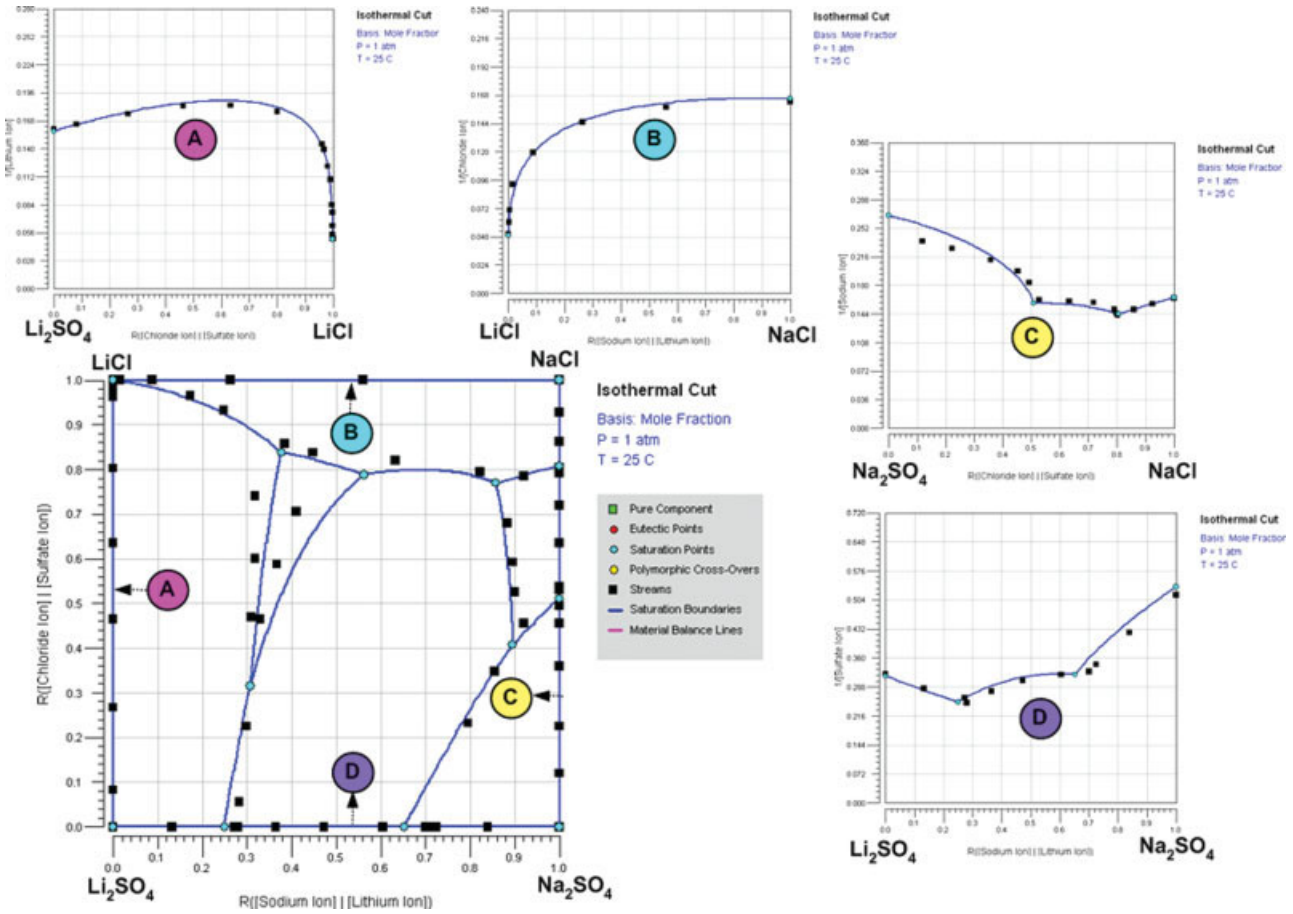

Figure 11. Comparison of calculated and experimental phase behavior for Na^+, Li^+//Cl^-, SO_4^{2-}- Water system.

Line - calculated phase behavior; Point - literature data.[25,50,53–55] [Color figure can be viewed in the online issue, which is available at www.interscience.wiley.com.]

mixture. These strategies are explained in Figure 3b for the case of $R(Li^+) = 0.7$.

Consider a mixture X shown in Figure 3b that has a solvent-less composition located in the lower right triangle of the base of the phase diagram. This mixture can be prepared by first adding a suitable mass of LiCl to Li_2SO_4 and then mixing it with an appropriate quantity of $MgSO_4{\cdot}7H_2O$ such that the $R(Li^+)$ value of the final mixture becomes 0.7. By adjusting the relative quantities of LiCl, Li_2SO_4, and $MgSO_4{\cdot}7H_2O$, other samples of solvent-less composition in the lower right triangle of the base can also be prepared for measurement. Now consider a mixture Y that has a solvent-less composition situated in the upper left triangle of the base. Here, we have to prepare it using LiCl, $MgCl_2{\cdot}6H_2O$ and $MgSO_4{\cdot}7H_2O$, as indicated in Figure 3b. For the special situation in which a mixture has its solvent-less composition lying on the diagonal joining the corners LiCl and $MgSO_4{\cdot}7H_2O$ of the base (mixture Z), only the two inorganic salts $MgSO_4{\cdot}7H_2O$ and LiCl are needed to prepare such a mixture.

Solubility measurements were performed for $R(Li^+)$ values of 0.55, 0.7, 0.85, and 1. The results are summarized in Table 4 and are displayed graphically in Figure 4. This figure is plotted by viewing the phase diagram from the face formed by the salts LiCl and Li_2SO_4 (the value of $R(Li^+)$ is used as a parameter). As can be seen, the solubility surface is relatively flat except for the region next to $R(Cl^-) = 1$. From the enlarged inset, we notice the existence of a discontinuity near $R(Cl^-) = 1$ for each of the saturation curves measured (points 1–4). Such a discontinuity on a solid–liquid saturation curve usually signifies a double saturation point of two different chemical species. Using the analytical method for some of the experimental points, the transition from $Li_2SO_4{\cdot}H_2O$ to $LiCl{\cdot}H_2O$ (for $R(Li^+) = 1$), $LiCl{\cdot}MgCl_2{\cdot}7H_2O$ (for $R(Li^+) = 0.85, 0.7$) or $MgCl_2{\cdot}6H_2O$ (for $R(Li^+) = 0.55$) was confirmed. The solid phases saturated at these discontinuous points are given in Table 5, where the point numbers correspond to those shown in Figure 4.

Experiments for $0 \leq R(Li^+) \leq 0.5$. In this region, the analytical method was used for measuring the solid–liquid equilibrium data. The strategy devised to prepare the samples is a little different from above. Initially, an aqueous mixture with $MgSO_4{\cdot}7H_2O$ and $Li_2SO_4{\cdot}H_2O$ in excess of their solubility limits was prepared. The solvent-less composition of this mixture was selected such that it was close to that of the

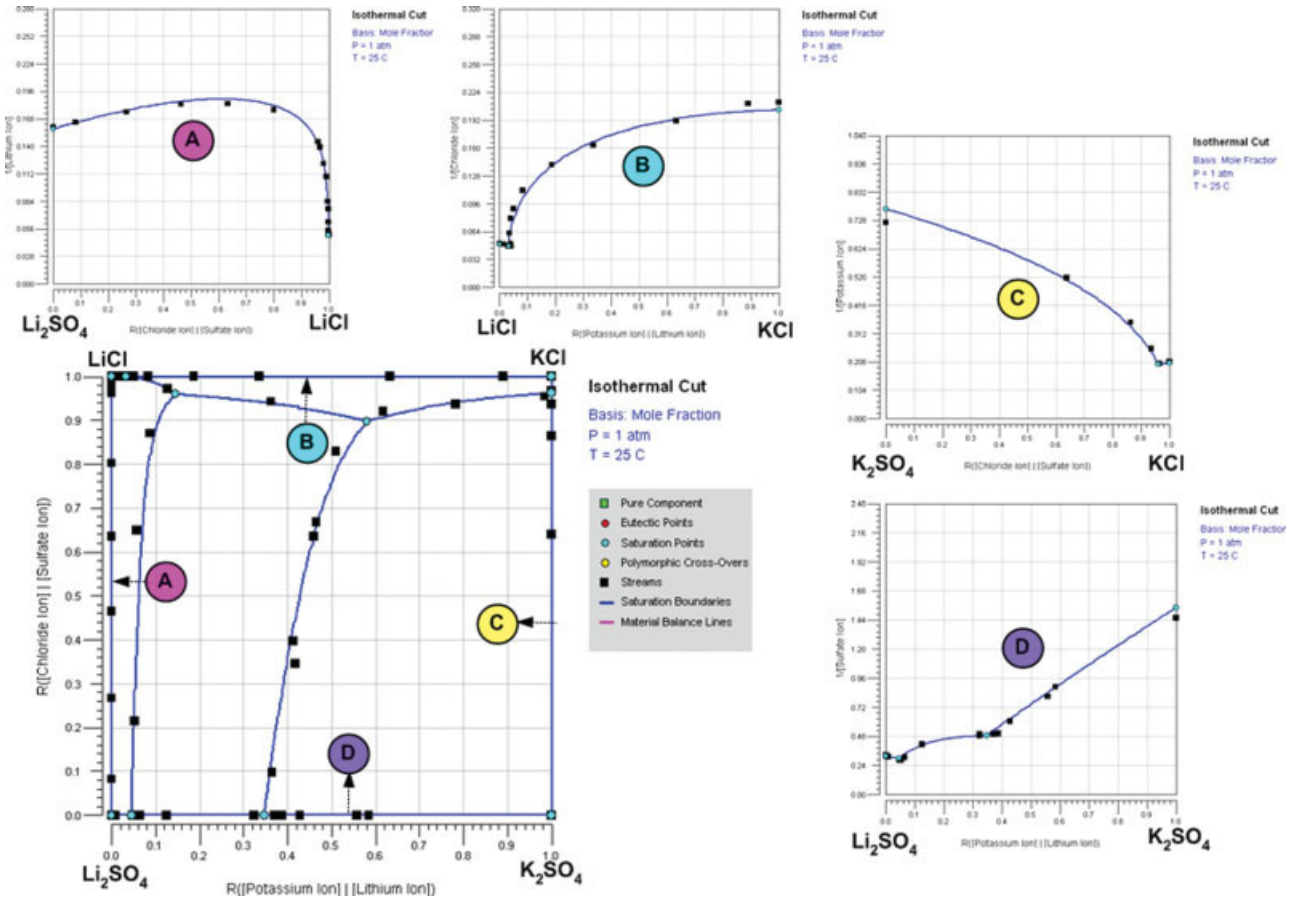

Figure 12. Comparison of calculated and experimental phase behavior for K^+, Li^+//Cl^-, SO_4^{2-}-Water system.

Line - calculated phase behavior; Point - literature data[26,50,53,56,57] [Color figure can be viewed in the online issue, which is available at www.interscience.wiley.com.]

double saturation point for salts $MgSO_4{\cdot}7H_2O$ and $Li_2SO_4{\cdot}H_2O$ on the plane of $R(Cl^-) = 0$ (i.e., the ternary system of Li_2SO_4-$MgSO_4$-H_2O). Then, a pre-determined amount of $MgCl_2{\cdot}6H_2O$ was added to the mixture to make up a sample of the desired $R(Cl^-)$ value. Other sample mixtures were prepared by using the same aqueous mixture of $MgSO_4{\cdot}7H_2O$ and $Li_2SO_4{\cdot}H_2O$ but with the addition of a different amount of $MgCl_2{\cdot}6H_2O$. This strategy is illustrated graphically in Figure 5.

The three sets of duplicated data points obtained for $0 \leq R(Li^+) \leq 0.5$ are tabulated in Table 6. The excellent agreements between the results of two identical experiments for each set of data verify the reproducibility of the analytical method. Figure 6 is a plot of such data points (points 10–12), which define the boundary between the crystallization regions of $MgSO_4{\cdot}7H_2O$ and $Li_2SO_4{\cdot}H_2O$. This boundary extends from the double saturation point of $MgSO_4{\cdot}7H_2O$ and $Li_2SO_4{\cdot}H_2O$ on the plane $R(Cl^-) = 0$ and curves towards the corner representing the salt $MgCl_2{\cdot}6H_2O$ as the value of $R(Cl^-)$ increases. Also included in the enlarged inset in Figure 6 are the double saturation points (points 1–4) determined for the region $0.5 \leq R(Li^+) \leq 1$ (Figure 4 and Table 5). The narrow crystallization regions for the chloride-containing salts underscore why there can exist a major source of uncertainty in the thermodynamic databases in the literature.

Additional Experiments. To check the consistency between the isothermal solid-disappearance method and the analytical method, the former technique was utilized to measure the saturation curve on the plane of $R(Li^+) = 0.4$. The results are listed in Table 4 and plotted in Figure 4. Similar to the saturation curves previously determined for planes of higher $R(Li^+)$ values, there also exists a discontinuous point near $R(Cl^-) = 1$ (point 5). But in addition to this, we find another discontinuous point at $R(Cl^-) = 0.54$ (point 6). This latter point was confirmed by analytical method as a double saturation point of $MgSO_4{\cdot}7H_2O$ and $Li_2SO_4{\cdot}H_2O$ (Table 5). When this data point is plotted in Figure 6, it fits in perfectly along the double saturation trough of $MgSO_4{\cdot}7H_2O$ and $Li_2SO_4{\cdot}H_2O$ obtained by the analytical method.

The isothermal solid-disappearance method was also employed to measure the solubility of the following three ternary subsystems of the Li^+, Mg^{2+}//Cl^-, SO_4^{2-} -H_2O system:

- Li^+, Cl^-, SO_4^{2-} -H_2O
- Li^+, Mg^{2+}, SO_4^{2-} -H_2O
- Li^+, Mg^{2+}, Cl^-, -H_2O

The experimental data acquired are recorded in Table 4. How they compare with the literature data[24,48–52] for each of

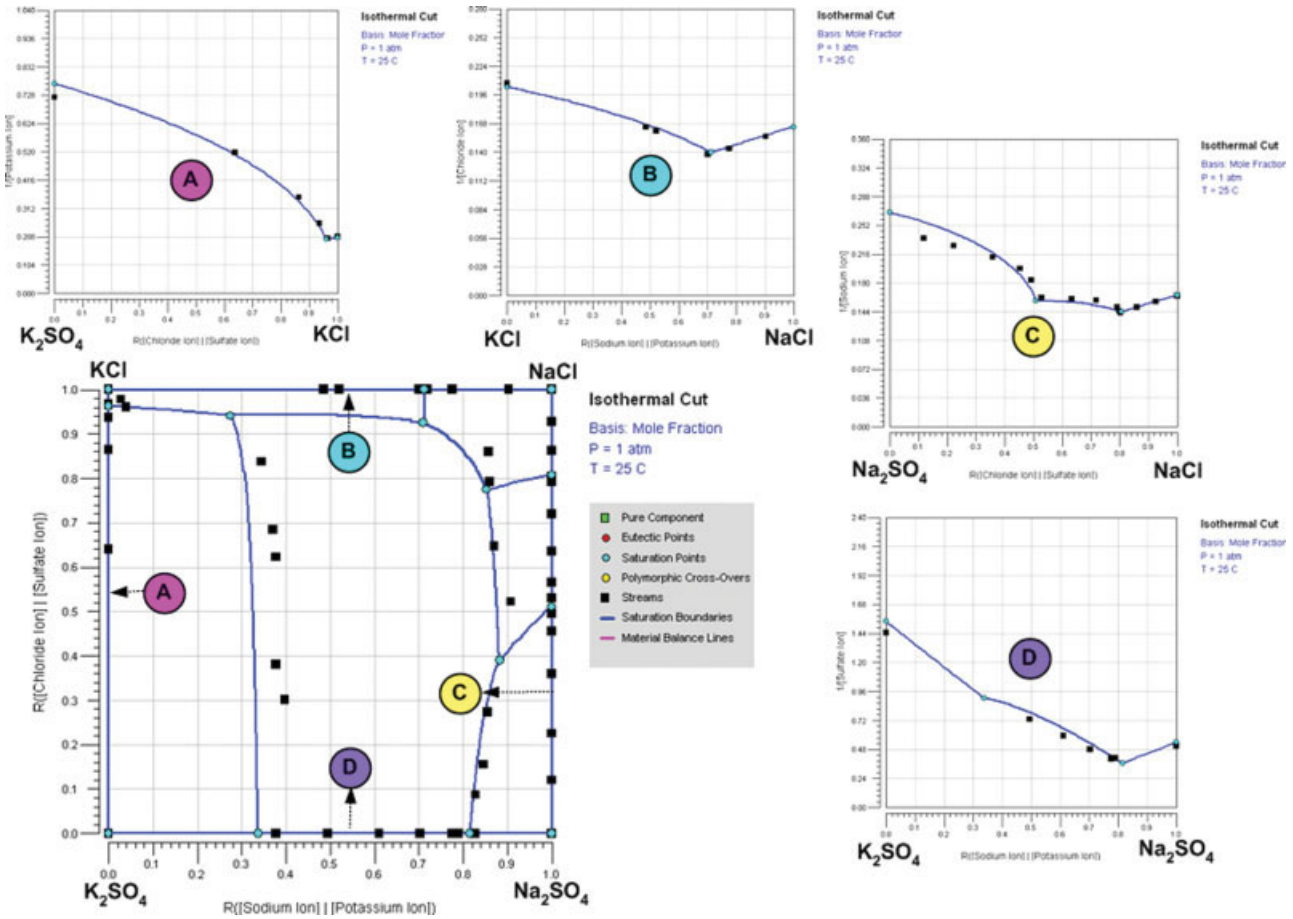

Figure 13. Comparison of calculated and experimental phase behavior for Na^+, K^+//Cl^-, SO_4^{2-}-Water system.

Line - calculated phase behavior; Point - literature data.[30,53] [Color figure can be viewed in the online issue, which is available at www.interscience.wiley.com.]

the ternary systems is presented in Figures 7–9 respectively. These experiments were performed early on in this study to verify the reliability of the isothermal solid-disappearance method and to gain insights into the phase behavior of the Li^+, Mg^{2+}//Cl^-, SO_4^{2-} -H_2O system. These insights led to the division of the composition space into two regions for solubility measurements.

Thermodynamic regression

For complete mathematical representation of the phase behavior of the model salt lake system, we need to estimate the solubility product parameters for each salt, UNIQUAC shape/size parameters for each ion, and the UNIQUAC binary interaction parameters for the aqueous phase species, based on all available experimental data. This estimation was performed by minimizing the objective function listed in Eq. 8 subject to the constraint outlined in Eq. 9:

$$F = \sum_{i \in \text{Data}} \left(w_i \frac{\ln K_{\text{sat}}^{\text{SP}}\big|_i - \ln K_{\text{sat}}^{\text{I}}\big|_i}{\ln K_{\text{sat}}^{\text{SP}}\big|_i} \right) \tag{8}$$

$$G = \sum_{i \in \text{Data}} \sum_{\substack{j \in \text{Salts} \\ j \neq \text{sat}}} \max\left(\ln K_j^I\Big|_i - \ln K_j^{\text{SP}}\Big|_i, 0.0 \right) = 0.0 \tag{9}$$

The objective function shown in Eq. 8 is based on the solubility criterion outlined in Eq. 1. For each data point, only the salts that are saturated are considered in evaluating the objective function. For each point, a weighting factor w_i is also used. The weighting factor is necessary due to large variations in the number of experimental data available for different subsystems of the salt lake system under consideration. These weighting factors were adjusted, between the values of 1 and 10, by trial-and-error to obtain a good representation for all parts and subsystems of the salt lake system.

The constraint shown in Eq. 9 reflects our desire that the regressed parameters should be such that, at each data point, the product of activities for all salts that are experimentally determined to be unsaturated remain less than their solubility products. This stability constraint is necessary in view of the large number of ions and salts in the salt lake system.

Tables 7 and 8 present the parameters obtained from regression. Table 7 lists the solubility products for all salts in

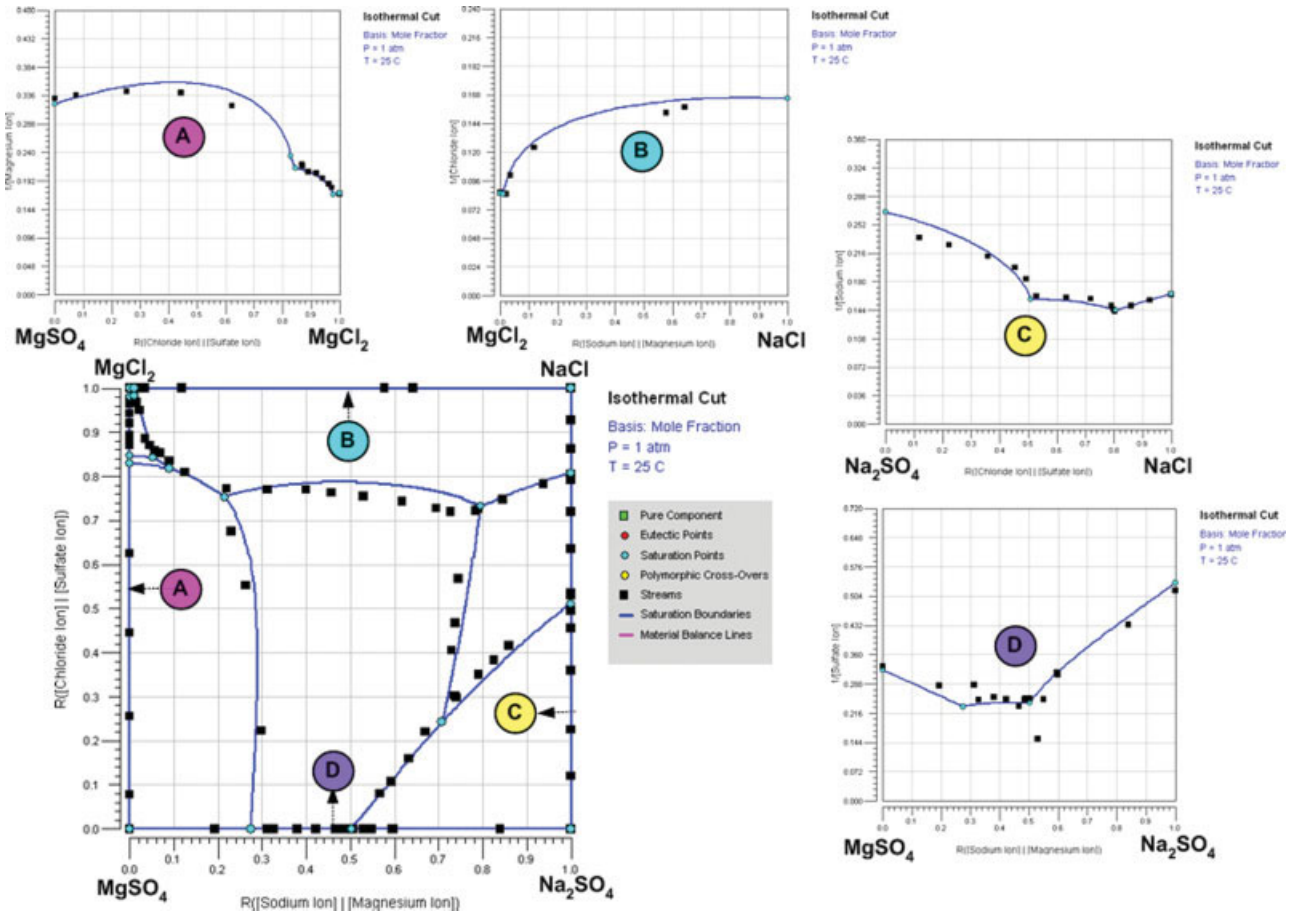

Figure 14. Comparison of calculated and experimental phase behavior for Na^+, Mg^{2+}//Cl^-, SO_4^{2-}-Water system.

Line - calculated phase behavior; Point - literature data.[42,44,53] [Color figure can be viewed in the online issue, which is available at www.interscience.wiley.com.]

the salt lake system and also the UNIQUAC shape/size parameters for all ions in the system. As noted earlier, the r and q parameters are regressed for the ions mainly for mathematical convenience, and their values for water are not regressed but are fixed at 0.92 and 1.40, respectively. The binary interaction parameters for all aqueous species are provided in Table 8. With these parameters, we now have the complete mathematical representation of the phase behavior for our salt lake system.

Visualization of phase behavior

Graphical visualization of phase behavior in the form of solid–liquid equilibrium phase diagram is an indispensable tool for the design and synthesis of crystallization-based separation processes. Phase diagrams translate the intangible phase behavior of chemical systems into visible pictorial features such as curves and surfaces. This provides an effective way for understanding the mutual relationship of the variables and the thermodynamic limits of the system under consideration. More importantly, with the insight derived from the visualization process, engineers can formulate a series of strategies and operations for carrying the feed mixture to the desired crystallization regions, where pure solids of the targeted components can be isolated. Such operations, which include temperature swing, solvent addition/removal etc, form a preliminary crystallization-based separation scheme and the corresponding process flowsheet can then be generated accordingly. Compared to the conventional methods that mainly rely on trial and error practice, process synthesis aided by phase diagrams is more reliable and requires less time, effort and resources.

Let us begin by visualizing some sample comparisons of the phase behavior calculated using the regressed parameters from Tables 7 and 8 and some of the experimental data from our collection. These comparisons are presented in Figures 10–15 for the six quaternary subsystems of the salt lake system and their constituent ternary subsystems.[25,26,30,31,42,44,50–57] A fairly good agreement between the calculated and experimental phase behavior can be observed. Each of the quaternary subsystems corresponds to a cut of the phase behavior taken with two out of the four cationic coordinates being set to zero. The resulting phase behavior is plotted as a solvent-less projection on the left-hand bottom corner of each figure. For example, the quaternary system in Figure 10 considers the Li^+, Mg^{2+}, Cl^-, and SO_4^{2-} ions only and corresponds to

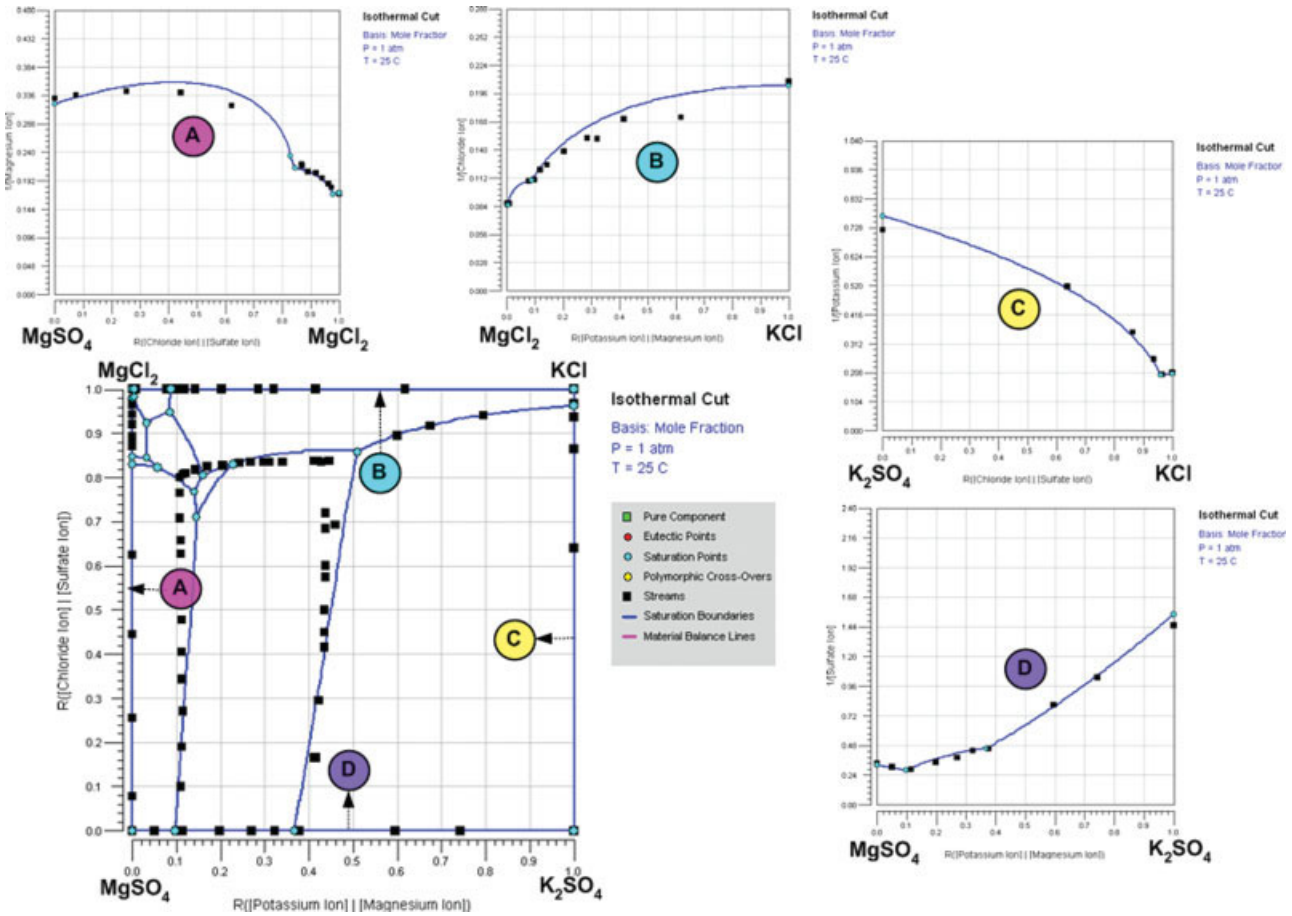

Figure 15. Comparison of calculated and experimental phase behavior for K^+, Mg^{2+}//Cl^-, SO_4^{2-}-Water system.

Line - calculated phase behavior; Point - literature data.[31,53] [Color figure can be viewed in the online issue, which is available at www.interscience.wiley.com.]

the cut of the complete phase behavior taken at $R(Na^+) = R(K^+) = 0$. As indicated on each figure, each ternary subsystem corresponds to the cut taken at each of the four edges of the quaternary phase diagram.

On the projections and cuts, the phase behavior is plotted as invariant points and saturation boundaries connecting these invariant points. The geometric varieties defined by these invariant points and the associated boundaries represent regions in the composition space in which one or more of the salts are saturated. Saturation varieties for one or more salts can thus be recognized by identifying the invariant points at which these salts are saturated and by tracing the boundaries that connect them. This information is useful in deciding which saturation varieties to avoid, which saturation varieties are desirable, and how to manipulate compositions to get to the desired saturation varieties, when synthesizing crystallization-based processes. Figure 16 shows three solvent-less two-dimensional projections of the quinary subsystem Na^+, K^+, Mg^{2+}//Cl^-, SO_4^{2-} -Water. In plotting these projections, compositions of both anions are considered. However, composition of one of the three cations is ignored for each of the projections as follows:

- Figure 16a ignores [K^+]
- Figure 16b ignores [Mg^{2+}]
- Figure 16c ignores [Na^+]

On each of these projections, the saturation region for the salt Astrakanite ($Na_2SO_4 \cdot MgSO_4 \cdot 4H_2O$) is highlighted. This region is defined by the invariant points at which Astrakanite is saturated and the boundaries connecting them. Any aqueous solution with composition that lies in this shaded region on all three projections is either saturated with Astrakanite or will become saturated with Astrakanite upon solvent (water) removal.

Visualization of phase behavior facilitates the tracking and understanding of the salt recovery process. As an example, consider two solar ponds with initial compositions listed in Table 9. The objective is to obtain lithium sulfate as monohydrate ($Li_2SO_4 \cdot H_2O$) by removing water at 25°C from these solar ponds. Figure 17 depicts the solvent-less projection for the Na^+, Li^+//Cl^-, SO_4^{2-} -Water subsystem of our salt lake system. Saturation varieties for $Li_2SO_4 \cdot H_2O$ and NaCl are shown as light and dark highlighted regions, respectively. Compositions for both solar ponds lie on the NaCl saturation variety. Therefore, removal of water from both ponds will first lead to crystallization of NaCl. Continued water removal, however, should eventually lead to the crystallization of lithium salts. Crystallization of NaCl in both solar ponds is shown on the

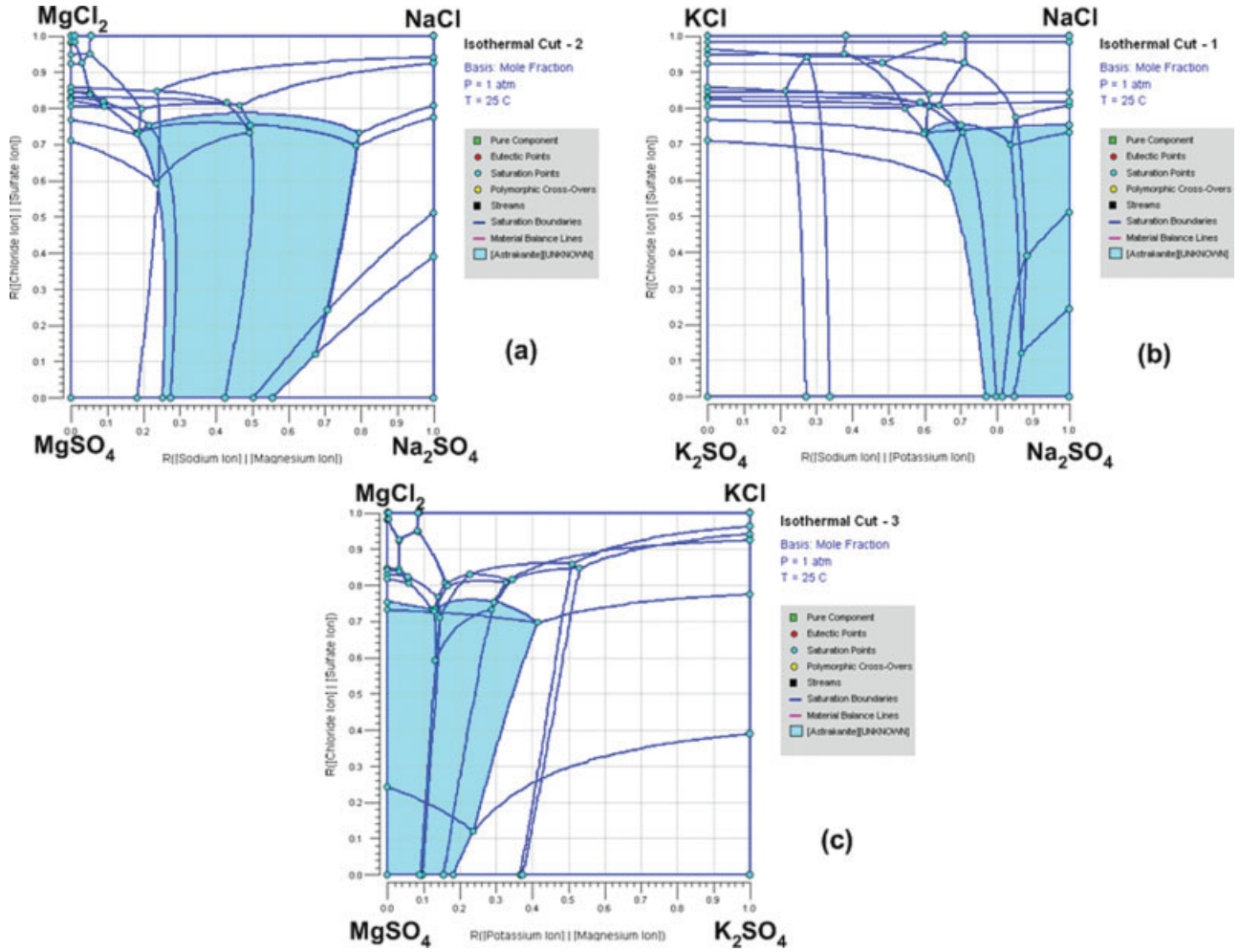

Figure 16. Two dimensional solvent-less projections for the Na^+, K^+, Mg^{2+}//Cl^-, SO_4^{2-}-Water system: (a) Projection ignoring [K^+]; (b) projection ignoring [Mg^{2+}]; (c) projection ignoring [Na^+].

Shaded area - saturation region for Astrakanite. [Color figure can be viewed in the online issue, which is available at www.interscience.wiley.com.]

phase diagram of Figure 17 by straight long-dashed lines connecting the original pond compositions and the NaCl invariant point. The pond compositions will move along these lines in the direction of the arrows as more and more NaCl is crystallized from the ponds due to water removal.

In case of Pond-I, with continued crystallization of NaCl, the pond composition will eventually hit the boundary separating the saturation varieties of NaCl and $Li_2SO_4{\cdot}H_2O$. From this point forward, the pond will crystallize both NaCl and $Li_2SO_4{\cdot}H_2O$ and the pond composition will move along this boundary as more water is removed. This is demonstrated in greater detail in Figure 18. Figure 18a shows the

Table 9. Initial Compositions of Solar Ponds (mass %)

Species	Pond-I (%)	Pond-II (%)
NaCl	16	16
$Li_2SO_4{\cdot}H_2O$	2	2
$LiCl{\cdot}H_2O$	10	1
Water	72	81

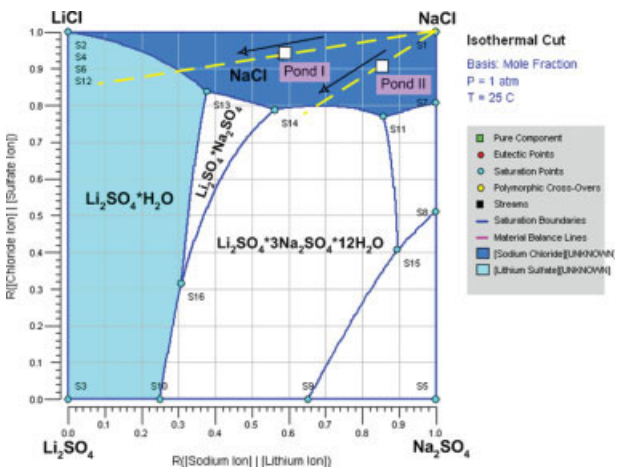

Figure 17. Operation of solar ponds involving the Na^+, Li^+//Cl^-, SO_4^{2-}-Water system.

[Color figure can be viewed in the online issue, which is available at www.interscience.wiley.com.]

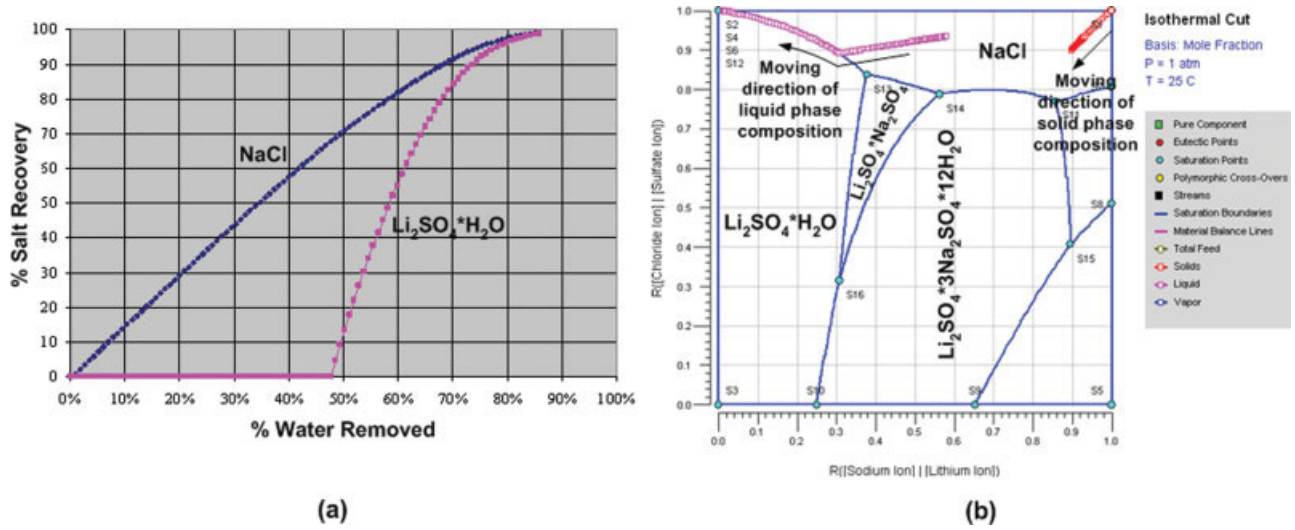

Figure 18. Operation of pond-I.

[Color figure can be viewed in the online issue, which is available at www.interscience.wiley.com.]

percentage recovery of salts from Pond-I as a function of water removal at 25°C and Figure 18b depicts the corresponding variation of the solids and liquid phase pond compositions on the phase diagram.

In case of Pond-II, however, the pond composition will first hit the boundary between NaCl and lithium double salt-1 ($Li_2SO_4{\cdot}3Na_2SO_4{\cdot}12H_2O$). Therefore, lithium sulfate will not immediately crystallize as monohydrate. Significantly more water has to be removed for obtaining lithium sulfate as monohydrate. Operation of Pond-II is shown in greater detail in Figure 19. Figure 19a shows the percentage recovery of salts from Pond-II as a function of water removal and Figure 19b presents the corresponding variation of the solids and liquid phase pond compositions on the phase diagram. As indicated in these figures, the liquid phase composition varies as follows:

- From NaCl saturation variety to the NaCl-lithium double salt-1 double saturation variety. During this period, only NaCl crystallizes in the pond.
- From the NaCl-lithium double salt-1 double saturation variety to the NaCl-lithium double salt-2 ($Li_2SO_4{\cdot}Na_2SO_4$) double saturation variety. During this period, lithium double salt-1 first crystallizes along with NaCl and then dissolves back into solution.
- From the NaCl-lithium double salt-2 double saturation variety to the NaCl-$Li_2SO_4{\cdot}H_2O$ double saturation variety. In this period, lithium double salt-2 first crystallizes along with NaCl and then dissolves back into solution.
- On the NaCl-$Li_2SO_4{\cdot}H_2O$ double saturation variety. Here $Li_2SO_4{\cdot}H_2O$ starts to crystallize along with NaCl.

Note that in cases where the crystals formed and the solution in the solar pond are not in equilibrium, the crystals of

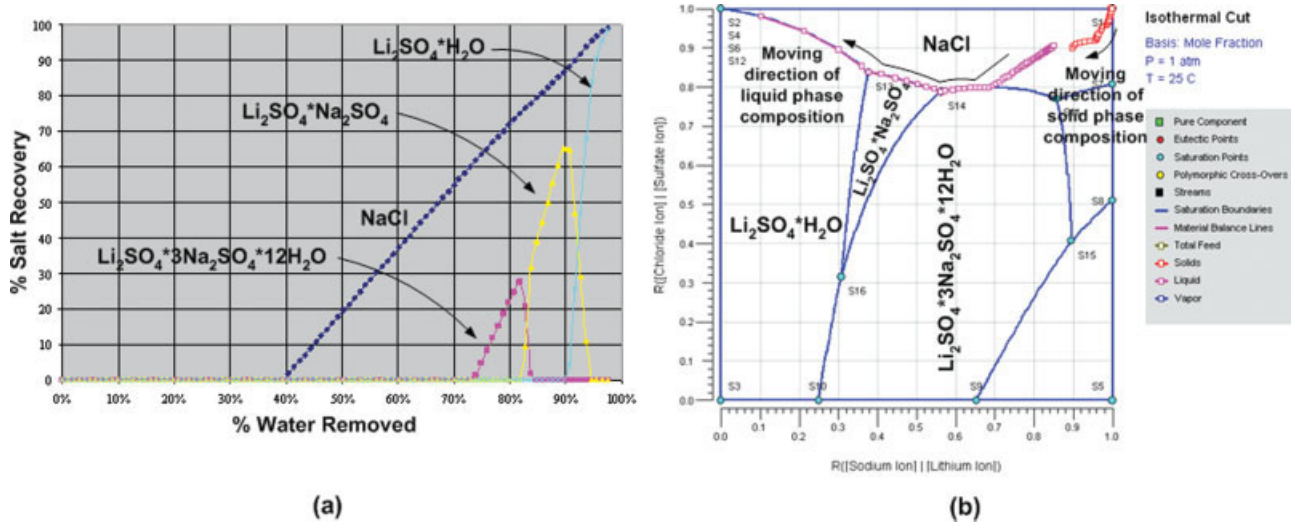

Figure 19. Operation of pond-II.

[Color figure can be viewed in the online issue, which is available at www.interscience.wiley.com.]

lithium double salt-1 ($Li_2SO_4 \cdot 3Na_2SO_4 \cdot 12H_2O$) and lithium double salt-2 ($Li_2SO_4 \cdot Na_2SO_4$) may not dissolve back into the solution.

As a result of this variation, the desired lithium sulfate monohydrate does not crystallize until ~90% of the water is removed from Pond-II, as opposed to ~48% for Pond-I

Conclusions

To utilize the rich resources in a salt lake in an optimal manner, it is highly desirable to fully understand its solid–liquid equilibrium thermodynamics. As demonstrated in a simple model aqueous system comprising Li^+, Na^+, K^+, Mg^{2+}, Cl^-, and SO_4^{2-} ions, the phase behavior can be highly complex. A large number of double salts and hydrates might exist, and some of them cram into a relatively small region of the composition space. Often, accurate data on solubility, presence of such compounds, and the size and location of crystallization regions simply do not exist. Even after experimentally determining such thermodynamic information, a table or a computer code might not be the most convenient vehicle for using such information. In process synthesis, it is highly desirable to be able to have a bird's eye view of the system under consideration. This article proposes an integrated approach consisting of representation, experimental determination and visualization to tackle this problem.

The heart of this approach is the high-dimensional phase diagram. Its dimensionality can be exactly defined once the cations and anions are specified. In actuality, this high-dimensional phase diagram is not plotted. Rather, it is broken down through cuts and projections into various low-dimensional subsystems. As long as these subsystems constitute a complete set and a sufficient amount of data is available, a thermodynamic model can be constructed with regressed model parameters to represent the high-dimensional phase diagram in its entirety. There are two advantages in going through this conceptual exercise. One is that it is easier to visually identify the missing data on a cut or projection. Another is that these cuts and projections can greatly enhance the design of experiments by identifying regions where additional data are needed to have the greatest impact on model accuracy and on process design. It is common that only part of the phase diagram is needed in detail in order to meet the objective of the process design project.

This integrated approach, when used together with the systematic procedures for crystallization-based process synthesis, forms a coherent set of tools that guides users all the way through from performing cuts on a multicomponent system to the synthesis and development of the associated crystallization-based process. All three elements of this approach go hand-in-hand. As demonstrated in this article, it is important that the compounds in the salt lake system be identified early in the project to ensure that they are represented in the thermodynamic model. The model parameters should be as simple as possible provided that the essential features are captured. In the course of this study, preliminary experiments were performed and additional measurements were made in various occasions to support the modeling effort.

This study is limited to aqueous systems at a fixed temperature. While only solar ponds are used in the initial stages of the process, separations further downstream might involve, for instance, organic solvents in drowning-out crystallization.[58] Thus, it is important that this study be extended to multiple solvents and other temperatures. Additional unit operations such as reactions, extraction and flotation should also be considered because the basic salts are often further processed to manufacture other products. Various commercial thermodynamic codes and high-throughput screening tools should also be considered to accelerate this integrated approach. Efforts in these directions are underway.

Acknowledgments

Financial support from the Research Grant Council (RGC grant no. 618106) is gratefully acknowledged. The authors thank Dr. K. D. Samant of ClearWaterBay Technology, Inc for his contribution at various stages of this work and specifically for regression of experimental data and visualization of phase behavior. These tasks were performed using the software tool SLEEK developed by ClearWaterBay Technology, Inc. In addition, KMN would like to thank L.A. Cisternas for arranging his industrial visit to Salar de Atacama, Chile. MET and LAC would like to thank CONICYT through the Regional Programme of Scientific and Technological Development, CICITEM.

Literature Cited

1. Arnold DS, Fairchild JL, Nichols DA, Coe MD. Process for producing sodium carbonate from complex brines. US Pat No 4,291,002; 1981.
2. Mehta VC. Process for recovering lithium from salt brines. US Pat No. 4,723,962; 1988.
3. Jongema P. Process of the precipitation of sodium chloride. US Pat No 5,221,528; 1993.
4. Efraim I, Lampert S, Holdengraber C. Co-production of potassium sulfate, sodium sulfate, and sodium chloride. US Pat. No. 5,552,126; 1996.
5. Wilkomirsky I. Production of lithium carbonate from brines. U.S. Pat No 5,993,759; 1999.
6. Lukes J. Process for obtaining monohydrated lithium sulfate from natural brines. U.S. Pat No 6,547,836 B1; 2003.
7. Berry DA, Ng KM. Separation of quaternary conjugate salt systems by fractional crystallization. *AIChE J*. 1996;42:2162–2174.
8. Wibowo C, Ng KM. Unified approach for synthesizing crystallization-based separation processes. *AIChE J*. 2000;46:1400–1421.
9. Schroer JW, Ng KM. Simplify multicomponent crystallization. *Chem Eng*. 2001;108:46–53.
10. Cisternas LA. Optimal design of crystallization-based separation schemes. *AIChE J*. 1999;45:1477–1487.
11. Cisternas LA, Torres MA, Godoy MJ, Swaney RE. Design of separation schemes for fractional crystallization of metathetical salts. *AIChE J*. 2003;49:1731–1742.
12. Cisternas LA, Cueto J, Swaney R. Flowsheet synthesis of fractional crystallization processes with cake washing. *Comput Chem Eng*. 2004;28:613–623.
13. Cisternas LA, Vasquez CM, Swaney RE. On the design of crystallization-based separation processes: review and extension. *AIChE J*. 2006;52:1754–1769.
14. Zemaitis JF Jr, Clark DM, Rafal M, Scrivner NC. *Handbook of Aqueous Electrolyte Thermodynamics: Theory and Application*. New York: AIChE, 1986.
15. OLI Systems, Inc. Available at: http://www.olisystems.com/. Accessed December 20, 2006.
16. Wibowo C, O'Young L, Ng KM. Streamlining crystallization process design. *Chem Eng Prog*. 2004;100:30–39.
17. Ma PH, Wang ZC, Xu G, Song ZH. Comprehensive exploitation of Ei Salar de Atacama salt lake. *J Salt Lake Sci*. 1998;6:61–66.
18. Torres MA, Cisternas LA, Galleguillos HR, Vargas PE. Determination of the Pitzer parameters for the solid-liquid equilibrium. *Ingeniería Química*. 2005;28:54–64.
19. Sander B, Fredenslund A, Rasmussen P. Calculation of vapor-liquid equilibria in mixed solvent/salt systems using an extended UNIQUAC equation. *Chem Eng Sci*. 1986;41:1171–1183.

20. Sander B, Fredenslund A, Rasmussen P. Calculation of solid-liquid equilibria in aqueous solutions of nitrate salts using an extended UNIQUAC equation. *Chem Eng Sci*. 1986;41:1197–1202.
21. Samant KD, Ng KM. Representation of high-dimensional solid-liquid phase diagrams for ionic systems. *AIChE J*. 2001;47:861–879.
22. Wibowo C, Ng KM. Visualization of high-dimensional phase diagrams of molecular and ionic mixtures. *AIChE J*. 2002;48:991–1000.
23. Wibowo C, Ng KM. Visualization of high-dimensional systems via geometric modeling with homogeneous coordinates. *Ind. Eng. Chem. Res*. 2002;41:2213–2225.
24. Silcock HL, editor. Solubilities of Inorganic and Organic Compounds, Vol. 3, Part 3. Oxford, England: Pergamon Press, 1979.
25. Ke-Yuan K. Temperature dependence of solubility in the quaternary reciprocal system Li^+, Na^+//Cl^-, SO_4^{2-}-H_2O Between 0°C and 100°C. *Russ J Inorg Chem*. 1960;5:92–96.
26. Campbell AN, Kartzmark EM, Lovering EG. Reciprocal salt pairs, involving the cations Li_2, Na_2, and K_2, the anions SO_4 and Cl_2, and water, at 25°C. *Can J Chem*. 1958;36:1511–1517.
27. Yanko AP. Symposium: "Physico-chemical analysis." (Fizikokhimicheskii analiz.) *Otd Akad Nauk SSSR Novosibirsk*. 1963;141.
28. Blasdale WC. Equilibria in solutions containing mixtures of salts. I. The system water and the sulfates and chlorides of sodium and potassium. *J Ind Eng Chem*. 1918;10:344–347.
29. Yanat'eva OK. *Izv Sektora Fiz-Khim Anal Akad Nauk SSSR*. 1949;17:373.
30. Rustamov PG, Bergman AG. *Zh Neorgan Khim*. 1958;3:2184.
31. Kurnakov NS, Luk'yanova EI. *Izv Akad Nauk SSSR Ser Khim*. 1938;1:41–42.
32. Kurnakov NS, Shoikhet DN. *Izv Sektora Fiz Khim Anal Akad Nauk SSSR*. 1938;10:310.
33. Solov'eva EF. *Tr Vses Nauch Issled Inst Gal*. 1953;27:67.
34. Van't Hoff JH, Meyerhoffer W. Sitzungsber. *Preuss Akad*. 1898;37.
35. Blasdale WC. Equilibria in solutions containing mixtures of salts. II. The system water and the chlorides and sulfates of sodium and magnesium at 25°C. *J Ind Eng Chem*. 1920;12:164–167.
36. Takegami S. *Mem Coll Sci Kyoto Imp Univ*. 1921;4:317.
37. Kurnakov NS, Zemcuznyj SF. *Z Anorg Allgem Chem*. 1924;140:149.
38. Leimbach G, Pfeiffenberg A. *Caliche*. 1929;11:64.
39. Kurnakov NS, Opykhtina MA. *Izv Inst Fiz Khim Anal Akad Nauk SSSR*. 1930;4:368–373.
40. Nikolaev VI, Burovaya EE. *Izv Sektora Fiz Khim Anal Akad Nauk SSSR*. 1938;10:248.
41. Rode T. *Izv Sektora Fiz Khim Anal Akad Nauk SSSR*. 1947;15:237.
42. Pel'sh AD. *Tr Vses Nauch Issled Inst Gal*. 1953;27:3.
43. Autenrieten H, Braun G. *Kali und Steinsalz*. 1960;3:15.
44. Autenrieten H, Braun G. *Kali und Steinsalz*. 1960;3:85.
45. Nývlt J. *Solid-Liquid Phase Equilibria*. Amsterdam, Netherlands: Elsevier Scientific, 1977.
46. Cohen-Adad R, Cohen-Adad MT. Solubility of solids in liquids. In: Hefter GT, Tomkins RPT, editors. *The Experimental Determination of Solubilities*. Wiley Series in Solution Chemistry, Vol. 6. Chichester, England: Wiley, 2003.
47. Mullin JW. *Crystallization*, 4th ed. Oxford, England: Butterworth Heinemann, 2001.
48. Druzhinin IG, Yanko AP. *Dokl Akad Nauk SSSR*. 1954;94:481.
49. Druzhinin IG, Yanko AP. *Tr Inst Khim Akad Nauk Krig SSR*. 1955;6:3.
50. Plyushchev VE, Tulinova VB. The LiCl-Li_2SO_4-H_2O system. *Russ J Inorg Chem*. 1959;4:536–538.
51. Voskresenskaya NK, Yanat'eva OK. *Izv Akad Nauk SSSR Ser Khim*. 1937;1:97.
52. Lepeshkov IN, Romashova NN. Salt solubility in the Li_2SO_4-Na_2SO_4-$MgSO_4$-H_2O system at 25°C. *Russ J Inorg Chem*. 1959;4:1301–1303.
53. Linke WF, Seidell A, editors. *Solubilities of Inorganic and Metal Organic Compounds*. Washington DC: American Chemical Society, 1965.
54. Ke-Yuan K. Solubility in the LiCl-NaCl-H_2O ternary system at 25°C, 50°C, 90°C and 100°C. *Russ J Inorg Chem*. 1960;5:90–92.
55. Ke-Yuan K. Solubility polytherm in the Li_2SO_4-Na_2SO_4-H_2O system. *Russ J Inorg Chem* 1959;4:864–868.
56. Plyushchev VE, Kuznetsova GP, Stepina SB. The LiCl-KCl-H_2O System. *Russ J Inorg Chem* 1959;4:652–654.
57. Campbell AN, Kartzmark EM. The systems Li_2SO_4-K_2SO_4-H_2O and Li_2SO_4-Na_2SO_4-H_2O. *Can J Chem*. 1958;36:171–175.
58. Taboada ME, Cisternas LA, Cheng YS, Ng KM. Design of alternative purification processes for potassium sulfate. *Ind Eng Chem Res* 2005;44:5845–5851.

Appendix: Extended UNIQUAC Model

Activity coefficients for the aqueous phase species are considered to have three contributions, viz., Debye–Hückel contribution, combinatorial contribution, and residual contribution.

The Debye–Hückel terms are:

$$\text{Water: } \ln\gamma_W^{D-H} = M_W \frac{2A^{D-H}}{b^3}\left[\left(1+bI^{1/2}\right) - \left(\frac{1}{1+bI^{1/2}} - \right)2\ln\left(1+bI^{1/2}\right)\right] \tag{A1a}$$

$$\text{Ions: } \ln\gamma_i^{*,D-H} = -z_i^2 A^{D-H}\left[\frac{I^{1/2}}{1+bI^{1/2}}\right]x_W \tag{A1b}$$

The terms involved are as follows:

M_W	Molecular weight of water (18.0153e-3 kg/mol)
x_W	Mole fraction of water
b	Model constant (1.5)
A^{D-H}	Debye–Hückel constant
I	Ionic strength
z_i	Charge on ion i

The following function of temperature is used for the Debye–Hückel constant for aqueous systems:

$$A^{D-H} = 1.131 + 1.335e^{-3}(T-273.15) + 1.164e^{-5}(T-273.15)^2 \tag{A1c}$$

The ionic strength is a function of molal concentrations of ions in the aqueous solution. It is calculated as:

$$I = \frac{1}{2}\sum_i z_i^2 [i] \tag{A1d}$$

Here $[i]$ represents molality of ion i.

The combinatorial terms are:

$$\text{Water: } \ln\gamma_W^{COMB} = \ln\left(\frac{\phi_W}{x_W}\right) + 1 - \frac{\phi_W}{x_W} - \frac{Z}{2}q_W\left[\ln\left(\frac{\phi_W}{\theta_W}\right) + 1 - \frac{\phi_W}{\theta_W}\right] \tag{A2a}$$

$$\text{Ions: } \ln\gamma_i^{*,COMB} = \left\{\ln\left(\frac{\phi_i}{x_i}\right) - \frac{\phi_i}{x_i} - \ln\left(\frac{r_i}{r_W}\right) + \frac{r_i}{r_W} - \frac{Z}{2}q_i\left[\ln\left(\frac{\phi_i}{\theta_i}\right) - \frac{\phi_i}{\theta_i} - \ln\left(\frac{r_i q_W}{r_W q_i}\right) + \frac{r_i q_W}{r_W q_i}\right]\right\}x_W \tag{A2b}$$

The terms involved are as follows:

r_i UNIQUAC volume parameter for component i

q_i UNIQUAC area parameter for component i

Z Coordination number (10)

In addition, the above equations use component volume and area fractions defined as follows:

$$\phi_i = \frac{x_i r_i}{\sum_j x_j r_j} \tag{A2c}$$

$$\theta_i = \frac{x_i q_i}{\sum_j x_j q_j} \tag{A2d}$$

Here x_i represents mole fraction of component i.

The residual terms are:

Water :

$$\ln \gamma_W^{\mathrm{RESID}} = q_W \left[1 - \ln \left(\sum_k \theta_k \tau_{kW} \right) - \sum_k \frac{\theta_k \tau_{Wk}}{\sum_l \theta_l \tau_{lk}} \right] \tag{A3a}$$

Ions :

$$\ln \gamma_i^{*,\mathrm{RESID}} = q_i \left[- \ln \left(\sum_k \theta_k \tau_{ki} \right) - \sum_k \frac{\theta_k \tau_{ik}}{\sum_l \theta_l \tau_{lk}} + \ln \tau_{Wi} + \tau_{iW} \right] x_W \tag{A3b}$$

Here all terms have their usual meanings. The only new terms are the energy parameters τ_{ij}. These parameters are expressed as a function of temperature as follows:

$$\tau_{ij} = \exp \left[- \frac{a_{ij} + b_{ij} T}{RT} \right] \tag{A3c}$$

Here, R is the universal gas constant and a_{ij} and b_{ij} represent the binary interaction parameters.

With these contributions, the activity coefficients for water and for the ionic species can be obtained as:

$$\text{Water:} \quad \ln \gamma_W = \ln \gamma_W^{\mathrm{D-H}} + \ln \gamma_W^{\mathrm{COMB}} + \ln \gamma_W^{\mathrm{RESID}} \tag{A4a}$$

$$\text{Ions:} \quad \ln \gamma_i^* = \ln \gamma_i^{*,\mathrm{D-H}} + \ln \gamma_i^{*,\mathrm{COMB}} + \ln \gamma_i^{*,\mathrm{RESID}} \tag{A4b}$$

Note that the activity coefficients for the ionic species are asymmetrically normalized and based on the molality scale. This is indicated by the superscript * and therefore molalities of ionic species are used in equations such as Eq. 1. The x_W term at the end of each contribution to the activity coefficients of ionic species reflects the conversion to the molality scale. In case of multiple solvents, this term should be replaced by:

$$\sum_s x_s \tag{A5}$$

Here the summation is over all molecular species in solution.

Manuscript received Feb. 7, 2007, and revision received Nov. 11, 2007.